Weather and Climate Extremes

Significant Tornado Environments In Canada Using ERA5-Derived Convective

--Manuscript Draft--

Manuscript Number:	
Article Type:	Research Paper
Keywords:	Tornado; Convective Storms; ERA5; Reanalysis; Convective Environments
Corresponding Author:	John Hanesiak University of Manitoba Winnipeg, Manitoba CANADA
First Author:	John Hanesiak
Order of Authors:	John Hanesiak
	Mateusz Taszarek
	David Walker
	Chun-Chih Wang
	Daniel Betancourt
Abstract:	This study uses ERA5 close-proximity soundings and associated convective parameters to characterize significant tornadic storm (F/EF2+) environments between 1980-2021 in parts of Canada. It was shown that ERA5 convective parameters are suitable to represent observed parameters, based on radiosonde comparisons. Results indicate that the eastern Prairies in western Canada have nearly double the LCLs with higher LFCs compared to eastern Canada (southern Ontario/Quebec). Central continental U.S. and Canadian regions appear to have the highest (most negative) convective inhibition. Central Canada (Manitoba) has the largest mixed-layer CAPE, then falls off to the west and east, mainly due to a combination of regional differences in low level moisture and steeper mid-level lapse rates in western Canada. Mean bulk wind shear and SRH increases from west to east, with eastern regions being significantly larger. Based on Bunkers storm motion, eastern Prairie tornadic storms are predicted to be the most deviant (right movers), with eastern Canada being the least deviant. Despite cold pool influences on tornadogenesis failure, western regions tend to have colder cold pools compared to eastern counterparts, based on the indices used. The supercell composite and significant tornado parameters are generally less than U.S. magnitudes, particularly in western Canada, and would require recalibration for more practical use in Canada. Overall, it appears that central and eastern Prairie significant tornadic storms are more dominated by thermodynamic influences compared to larger kinematic influences in eastern regions.
Suggested Reviewers:	Harold Brooks harold.brooks@noaa.gov Dr. Brooks is an expert in severe convective weather and tornadoes.
	Tammy Weckwerth tammy@ucar.edu Dr. Weckwerth has expertise in severe convective weather, including hazards such as tornadoes.
	Stephen Dery stephen.dery@unbc.ca Dr. Dery has broad expertise in extreme weather and hydrological events.

Department of
Environment and Geography

Winnipeg, Manitoba
Canada R3T 2N2
Telephone (204) 474-9667
Fax (204) 474-7699
environment_geography@umanitoba.ca

April 24, 2023

Dr. John Hanesiak
Professor
Centre for Earth Observation Science
440 Wallace Bldg.
University of Manitoba
Winnipeg, MB, Canada R3T 2N2
204-474-7049
john.hanesiak@umanitoba.ca

Editors
Weather and Climate Extremes
Elsevier Publishing

Dear Editors,

We are pleased to submit our research article titled "**Significant Tornado Environments In Canada Using ERA5-Derived Convective Parameters"** for publication in Weather and Climate Extremes, by J. Hanesiak, M. Taszarek, D. Walker, C-C Wang and D. Betancourt. The article has not been submitted to any other journal or published in other journals. Only one PDF was submitted that contains all of the relevant information, no supplemental material was used.

Motivation: There have been no formal studies focused on tornado environments across Canada and their regional comparisons, even though Canada experiences major tornado events. Our work attempts to fill a gap in this knowledge to assist weather forecasters as well as building Canadian climatologies.

Contributions: For the first time in Canada, we provide a quantitative guide for commonly used meteorological parameters and diagrams that are associated with significant tornadoes, and how these vary across different regions in Canada. We also compare our results to other regions of the World, such as, the U.S., Europe and China, to put Canada into international context.

Impact: Our results are important for better understanding strong tornado environments in Canada with the goal of (1) providing operational meteorologists with insight into the primary meteorological parameter magnitudes associated with strong tornadoes, to assist in weather forecasting, and (2) adding to the climatological body of knowledge of extreme weather events in Canada.

Suggested Reviewers:

Dr. Harold Brooks, NSSL (harold.brooks@noaa.gov)

Dr. Stephen Dery, University of Northern British Columbia (stephen.dery@unbc.ca)
Dr. Tammy Weckwerth, NCAR (tammy@ucar.edu)

Feel free to reach out to me via email, if you require any further information. We look forward to future correspondence.

Sincerely,

Dr. John Hanesiak

Significant Tornado Environments In Canada Using ERA5-Derived Convective Parameters

John Hanesiak,[a] Mateusz Taszarek,[b] David Walker,[a] Chun-Chih Wang[a] and Daniel Betancourt[a]

[a] *Centre for Earth Observation Science, Department of Environment and Geography, University of Manitoba, Winnipeg, MB, Canada*

[b] *Department of Meteorology and Climatology, Adam Mickiewicz University, Poznan, Poland*

Corresponding Author:
Dr. John Hanesiak
john.hanesiak@umanitoba.ca
Centre for Earth Observation Science (CEOS)
440 Wallace Bldg., 125 Dysart Road,
University of Manitoba
Winnipeg, Canada, R3T 2N2

Submitted to Weather and Climate Extremes

Tuesday April 25, 2023

KEYWORDS: Tornado; Convective Storms; ERA5; Reanalysis; Convective Environments; CAPE

Competing Interests Statement: None of the authors have conflicts of interest and all material provided was produced by the authors.

Author contributions: J. Hanesiak was responsible for conceptualization, formal analysis, methodology, writing/editing content, funding; M. Taszarek was responsible for data curation, analysis, data analysis tools, visualization, review/editing content, funding; D. Walker was responsible for statistical methodology, data analysis/tools, visualization, writing/editing/reviewing content; C-C Wang was responsible for data analysis/tools, visualization and reviewing/editing content; D. Betancourt was responsible for reviewing scientific content, reviewing/editing text.

ABSTRACT

This study uses ERA5 close-proximity soundings and associated convective parameters to characterize significant tornadic storm (F/EF2^{+}) environments between 1980-2021 in parts of Canada. It was shown that ERA5 convective parameters are suitable to represent observed parameters, based on radiosonde comparisons. Results indicate that the eastern Prairies in western Canada have nearly double the LCLs with higher LFCs compared to eastern Canada (southern Ontario/Quebec). Central continental U.S. and Canadian regions appear to have the highest (most negative) convective inhibition. Central Canada (Manitoba) has the largest mixed-layer CAPE, then falls off to the west and east, mainly due to a combination of regional differences in low level moisture and steeper mid-level lapse rates in western Canada. Mean bulk wind shear and SRH increases from west to east, with eastern regions being significantly larger. Based on Bunkers storm motion, eastern Prairie tornadic storms are predicted to be the most deviant (right movers), with eastern Canada being the least deviant. Despite cold pool influences on tornadogenesis failure, western regions tend to have colder cold pools compared to eastern counterparts, based on the indices used. The supercell composite and significant tornado parameters are generally less than U.S. magnitudes, particularly in western Canada, and would require recalibration for more practical use in Canada. Overall, it appears that central and eastern Prairie significant tornadic storms are more dominated by thermodynamic influences compared to larger kinematic influences in eastern regions.

1. Introduction

On average in any given year, Canada can experience 60 (based on actual reports) to 230 (based on modeling) tornadoes (Newark 1984; Sills et al. 2012; Cheng et al. 2013), resulting in multi-millions of dollars in damage and loss of life (e.g. Sills et al. 2012; Cheng et al. 2013). The Barrie 1985 (Etkin et al. 2001) and Edmonton 1987 (Bullas and Wallace 1988; Charlton et al. 1995) tornadoes are a couple examples of the most costly and significant events in Canadian history. More recent examples include the 2021 Barrie region tornadoes (CAD 100 million) and 2018 Ottawa-Gatineau tornadoes (CAD 295 million) (Insurance Bureau of Canada 2018, 2021).

Despite their impacts in Canada, there have been limited studies to better understand tornadic storm mesoscale environments, primarily due to a lack of data. Some related early field work was Chisholm and Renick (1972) who distinguished single-cell, multi-cell and supercell environments based on hodographs, however, the main focus was hailstorms. Strong (1979, 1986) began the development of an Alberta severe storm conceptual model, then Smith and Yau (1993a,b) used Limestone Mountain Experiment (LIMEX-85; Strong 1989) field data to create an Alberta severe convective outbreak conceptual model. Combined results from these studies focused on synoptic setting, boundary layer and capping evolution, horizontal moisture flows and mountain-plains circulation role in convection initiation. Some of the results can apply to tornadic storms, however, most of the field sampling was tailored to hailstorms.

Duplika and Reuter (2006a,b; 2011) summarized various convective settings to storm severity, including tornadic storms in central Alberta, using one operational radiosonde site. They suggested the degree of low level veering, along with storm relative helicity (SRH), were associated with stronger tornadic storms; thresholds were 0-3 km SRH > 150 $m^2 s^{-2}$ and 900–500 mb shear exceeding 3 $m s^{-1} km^{-1}$ for F2-F4 tornadoes, which are smaller than typical U.S. environments (e.g. Thompson et al. 2003). Dyck et al. (2014) used close proximity radiosondes to compare an EF0 and EF1 tornado environments during the 2008 Understanding Severe Thunderstorms and Alberta Boundary Layers Experiment (UNSTABLE; Taylor et al. 2008). Higher low level SRH, deeper boundary layer depth and moisture (lower lifted condensation level (LCL) and level of free convection (LFC) occurred for the EF1 event.

A relation between lake breezes and tornado climatology in Ontario, Canada was inferred with limited data (King et al. 1996; King 1997); Ontario lake breezes can initiate convection, but may also play a role in tornadogenesis via lake breeze-storm interactions (e.g. King et al. 2003).

Sills and King (2000) looked at landspout tornadoes generated by coincident misovortices and growing convective towers along lake breeze boundaries, however, cases were limited and only applied to non-mesocyclone events.

Some of the above studies were synoptic scale in nature while others were case studies and not able to analyze "general" mesoscale characteristics of tornadic events. Most of the studies are also very geographically focused, for example, Alberta.

Severe convective and tornadic storms mesoscale environments have been studied outside of Canada, using close-proximity model or reanalysis soundings. The reader is referred to Taszarek et al. (2020) and Coffer et al. (2020) for a review with only limited discussion here, focused on tornadic storms. Examples of early work include Brooks et al. (2003) and Thompson et al. (2003) who used model and reanalysis-derived convective parameters to characterize tornadic environments. Shortly after, newer model and reanalyses datasets were used to further advance knowledge, make comparisons amongst U.S. regions and convective modes (e.g. Grams et al. 2012; Thompson et al. 2007, 2012, 2013; Anderson-Frey et al. 2016, 2018, 2019; Coffer et al. 2019; Gensini et al. 2019, 2021). All studies pointed to the importance of various convective available potential energy (CAPE) and wind shear layers, including low level SRH.

Taszarek et al. (2020) (hereafter T2020) compared European and U.S. convective environments, including tornadoes, using ERA5 (Hersbach et al. 2020) and found that the U.S. has higher moisture, CAPE, convective inhibition (CIN), wind shear, and mid-tropospheric lapse rates, whereas, Europe has higher 0–3-km CAPE and low-level lapse rates. They also noted that (1) WMAXSHEAR (square root of 2 times CAPE multiplied by 0–6 km wind shear) represents significant severe thunderstorm severity fairly well, and (2) supercell composite parameter (SCP) and significant tornado parameter (STP) typically produce better forecasts over the U.S.. Coffer et al. (2020) also used ERA5 to show that 0 - 500 m SRH can be useful for tornado prediction in the U.S. and Europe, however, 100 - 200 m SRH layers were the most skillful in Europe. A recent ERA5 study comparing China and U.S. strong tornado (F/EF2^{+})[1] events suggested that China has less favorable kinematic conditions than the U.S., which partially explains its less frequent strong tornado events (Zhang et al. 2023).

[1] F/EF2^{+} (strong tornadoes) refers to tornado events producing ≥ F2 or EF2 damage according to the original Fugita (F) scale and enhanced Fugita (EF) scale; see Doswell et al. (2009) and Edwards et al. (2013) for historical background, scale comparisons and U.S. implementation information.

The objective of this article is to characterize significant tornado (F/EF2$^+$) environments using ERA5 in parts of Canada, and regionally compare them. Brief comparisons to the U.S., Europe and China are also made. The broader goal is to provide knowledge of "typical" significant tornado environments, and their variations, to contribute to prediction capabilities and associated climatology. The characterization involves examining thirty-five convective parameters derived from ERA5 model-level vertical profiles important to describe tornadic environments, similar to, Grams et al. (2012), Gensini and Brookes (2018), Anderson-Frey et al. (2016), but will closely follow T2020 since this study uses a similar, but expanded, ERA5-derived convective parameter dataset that were processed with the same computational script.

This article is organized by data and methods (Section 2) describing the study area, various datasets used, a brief ERA5 convective parameter validation, and statistical analysis methods. Section 3 contains the main results, focusing on provincial tornadic storm environments for various thermodynamic, kinematic and composite parameters, as well as composite thermodynamic and wind profiles. Section 4 concludes by summarizing the key findings, limitations of the work, and future research.

2. Data and Methods

2.1 Tornado Data and Study Area

This study used F/EF2$^+$ tornado events from the Canadian tornado database between 1980 - 2009 (Sills et al. 2012) (https://open.canada.ca/data/en/dataset/fd3355a7-ae34-4df7-b477-07306182db69) and 2010 - 2020 data made available by the Northern Tornadoes Project (NTP; https://www.uwo.ca/ntp/), that included some source data from Environment and Climate Change Canada. Relevant to this study, data included: (1) date and time of tornado, (2) nearest town/city and province, (3) approximate latitude/longitude of tornado, (4) F/EF rating. Canada began using the EF-scale in April 2013 (Sills et al. 2014) and was implemented in the database. Although difficult to quantify, errors associated with the F/EF scale transition are not expected to be significant for F/EF2$^+$ events; <2% increases (shifts) in F2$^+$ from F to EF scales (Edwards et al. 2021).

Most of the significant tornadoes (defined as F/EF2⁺) occurred between Alberta and Quebec, thus, the focus is on 5 provinces; Ontario was divided into northern (west of 85° W) and southern (east of 85° W) regions due to: (1) its vast size longitudinally, where storm environments may be different, and (2) the tornado "gap" north and northeast of Lake Superior (Fig. 1 and Cheng et al. 2013). Abbreviated region names are used hereafter. Subdividing other provinces was not done due to limited tornado samples that can affect statistical comparisons. Grouping tornado events by provincial regions was done to simplify the analysis, but still allows for reasonable environment assessments based on the authors' experience. Future work will examine cluster analysis or machine learning to group Canadian tornado events.

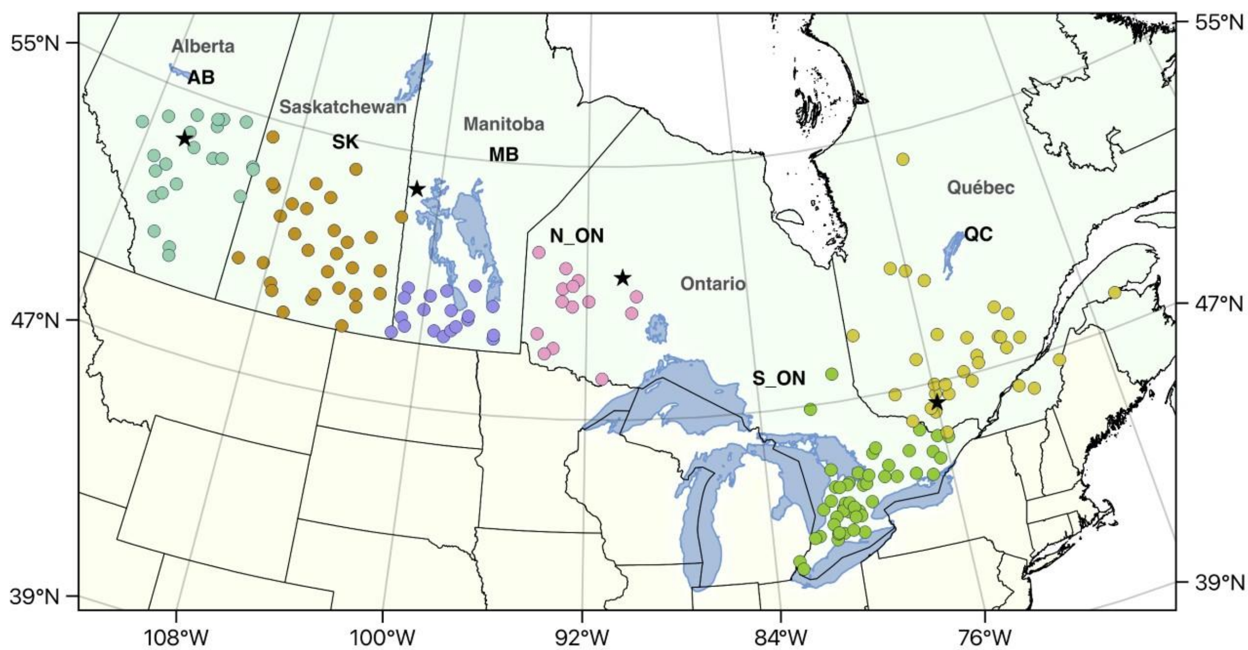

Figure 1: Geographic map of the study area, including full and abbreviated provincial names and territorial boundaries. Circles represent the 1980 - 2020 166 F/EF2$^+$ tornado events used in this study; 23 in AB, 31 in SK, 19 in MB, 14 in N_ON, 48 in S_ON, and 31 in QC. N_ON is defined as > 85° W. The 4 operational radiosonde sites used in Section 2.2 are indicated (filled stars); from west to east, Stoney Plain, AB (WSE 71119), The Pas, MB (YQD 71867), Pickle Lake, ON (WPL 71845), and Maniwaki, QC (WMW 71722).

There were 211 F/EF2$^+$ tornadoes between 1980 - 2020[2] with 35 days of multiple (two or more) significant tornadoes; 5 days in AB, 4 in SK, 4 in MB, 2 in N_ON, 11 in S_ON and 9 in

[2] More than 211 F/EF2$^+$ tornado events occurred, however, several cases did not have sufficient information (e.g. date and/or time) in the tornado database.

QC. To minimize environmental statistical oversampling, Potvin et al. (2010) was used, who suggested a Goldilocks-zone (GZ) for optimal proximity soundings to be within 1-2 h and 40-80 km of the actual tornado. Therefore, only the highest F/EF-rated occurrence was kept in the analysis for any multi-tornado day, unless other tornadoes were > 80 km *or* more than 2 h from the highest F/EF-rated event. If two or more tornadoes had the equivalent highest-rated rank on any day, and occurred within the GZ of one another, then only one of those tornadoes was randomly selected to "represent" the environment. After applying these criteria, a total of 166 F/EF2^{+} cases with unique ERA5 profiles were used in the analysis (45 were removed to minimize oversampling and avoid duplicated profiles), with 23 cases in AB, 31 in SK, 19 in MB, 14 in N_ON, 48 in S_ON, and 31 in QC (Table 1; Fig. 1). 84% were F/EF2, while 12% were F/EF3, with only 6 F/EF4 cases (Table 1). The only F/EF5 in Canadian history occurred 22 June 2007 in Manitoba. Between 1980 - 2020, N_ON (MB) did not have any recorded cases prior to 1994 (1984), while SK and AB first cases were 1982 and 1981, respectively; causes for these differences may be real, or due to a lack of reports or problematic reports that were filtered out of the national database.

Scale	**Canada**	**AB**	**SK**	**MB**	**N_ON**	**S_ON**	**QC**
F/EF2	139	18	26	13	14	41	27
F/EF3	20	4	5	3	0	4	4
F/EF4	6	1	0	2	0	3	0
F/EF5	1	0	0	1	0	0	0
TOTAL	**166**	**23**	**31**	**19**	**14**	**48**	**31**

Table 1: Regional distribution of 1980 - 2020 F/EF2^{+} Canadian tornado events used in this study for: Alberta (AB), Saskatchewan (SK), Manitoba (MB), northern Ontario (N_ON), southern Ontario (S_ON) and Quebec (QC).

2.2 ERA5 Convective Parameters and Validation

Similar ERA5 data (Hersback et al. 2020) and derived convective parameters were used as T2020, so an abbreviated discussion is provided. The rationale for using ERA5 hybrid-sigma levels is that: (1) ERA5 represents North American and European convective environments reasonably well (Taszarek et al. 2021; hereafter T2021), and (2) direct comparisons between other ERA5 studies can be made. Important ERA5 aspects include (Hersbach et al. 2020): (1) 0.25° (~31 km) horizontal resolution, (2) 137 terrain-following hybrid-sigma levels including 28 levels in the lowest 2 km for improved boundary layer representation (better compared to interpolated pressure levels commonly used in other studies), and (3) hourly temporal resolution.

ERA5 vertical profiles were collected for each of the 166 F/EF2$^+$ tornadoes as close as spatially and temporally as possible (time = 0; T0) to actual events, including within ± 4 h of T0; 9 profiles per tornado event (T-4, T-3, ..., T0, …, T+3, T+4). Manual profile inspection was performed for each to ensure temporal errors were minimized; for example, if the ERA5 timing of convective precipitation (storm) was not accurate, this would potentially affect the T0 profile and lead to its contamination by simulated precipitation (King and Kennedy 2019). The "representative" pre-convective profile was selected primarily based on boundary layer evolution (e.g. combination of maximum near-surface temperature timing and/or any obvious signs of cold pool contamination) between T-4 to T+4 of each tornado event. This led to ~95% of the representative profiles to be within ± 2 h of tornado occurrence (most were either T-2, T-1 or T0), with no T-4 or T+4 profiles used. Multiple profiles (i.e. grid points) in space were not considered since the selection of representative profiles in time would potentially alleviate some of the ERA5 spatial errors, and averaging several grid-point profiles to represent the environment (instead of one single profile) could overly smooth the profile. The drawback of not explicitly accounting for ERA5 spatial errors is that one assumes ERA5 storms are at least within reasonable distance (e.g. ~80 km) to the actual storm. It is unknown if this criteria was met for every tornadic storm.

This study used thundeR v.1.1 (Taszarek et al. 2023) to generate all ERA5-derived convective parameters, similar to, but larger number of parameters than T2020. However, the focus included 35 parameters that have been linked to tornadic storms (Appendix A). Only some parameters showed Canadian regional differences.

Although T2021 conducted ERA5 validation over North America, only limited detail was available for Canada. There are only four Canadian sounding sites within the domain of interest (see Fig. 1). The validation is not meant to be exhaustive, but nonetheless, is important to ensure convective parameter confidence. Moosonee, ON was not included due to its proximity to James Bay that could pose local environment variations, and since no strong tornadoes occurred in this area.

Comparisons were made between convective parameters derived from the four operational sounding sites and nearest ERA5 grid point soundings, similar to T2021. Operational sounding data between 1990 - 2020 from the University of Wyoming were used (http://weather. uwyo.edu/upperair/). Stringent quality-control was applied to the operational soundings to remove incomplete, unphysical or error-prone soundings following the same methodology as T2021. Only time periods between 1800 - 0000 UTC May 1 - September 30 were investigated, to coincide with the majority of the convective season and convective “daytime”. As a result, 16,005 rawinsonde measurements were compared with ERA5 profiles over the 30 year period. Several selected convective parameters were calculated for the operational and coincident ERA5 soundings along with various statistical error metrics (Fig. 2 - 4 and Tables 2 - 3). All comparisons included soundings that had 0 - 500 m mixed-layer (ML) CAPE (ML_CAPE) > 0 J kg^{-1}. Emphasis was placed on ML parcels, as opposed to most-unstable (MU) parcels, since T2021 found better correlations for ML parcels; it turned out that results here were similar in most cases (not shown).

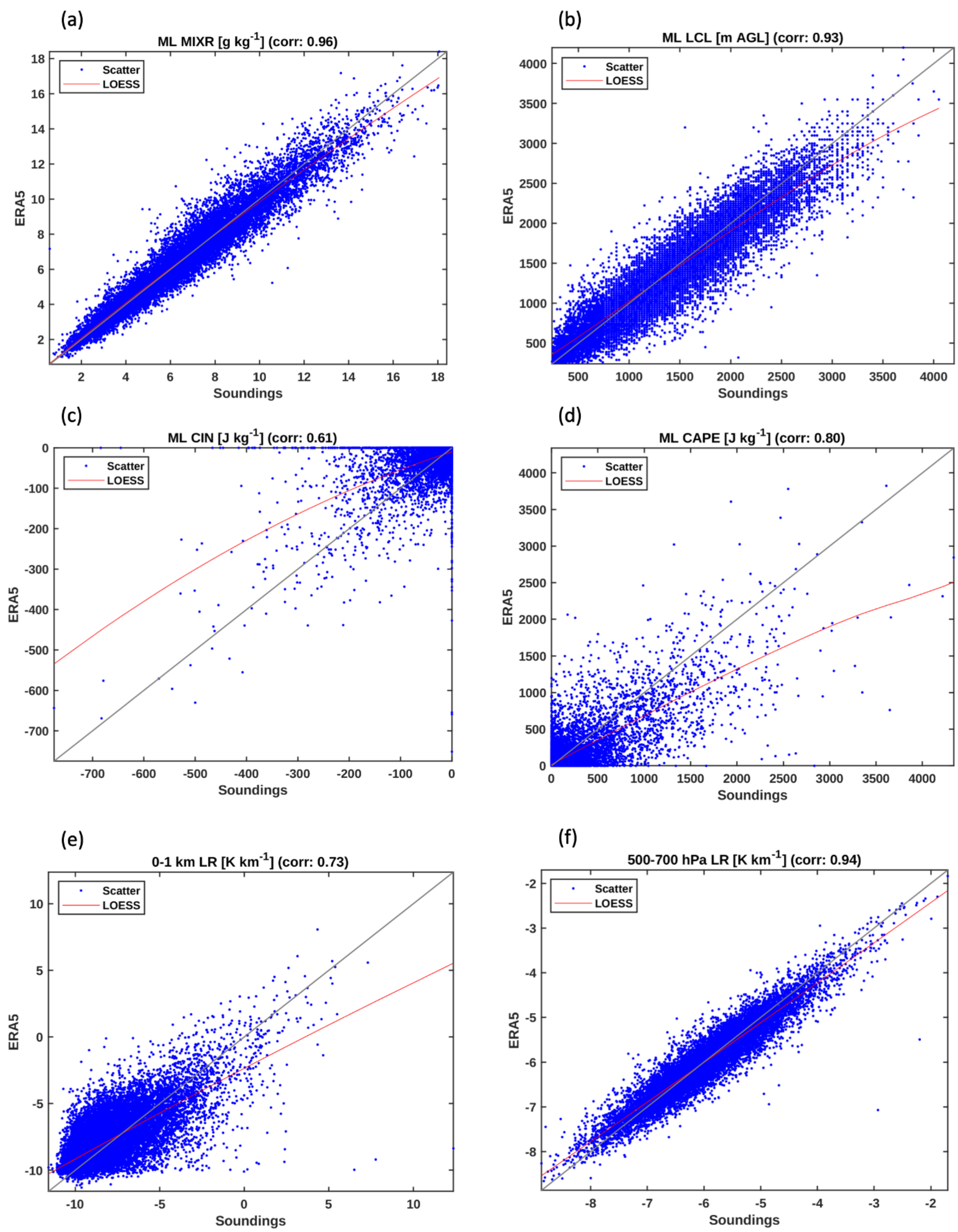

Figure 2: Scatter plots of selected parcel and thermodynamic parameters error comparisons between operational observed soundings and collocated ERA5 proximity profiles for (a) mixed-layer mixing ratio (g kg^{-1}), (b) mixed-layer lifted condensation level (m), (c) mixed-layer convective inhibition (J kg^{-1}), (d) mixed-layer CAPE (J kg^{-1}), (e) 0–1 km lapse rate (K km^{-1}), (f) 500–700 hPa lapse rate (K km^{-1}). One-to-one ratio (black line) and locally estimated scatterplot smoothing (LOESS) (red line) are shown. The Pearson correlation coefficient is indicated at the top of each plot.

Analysis revealed that the ERA5-derived convective parameters replicated observed parameters fairly well in most cases, with similar errors as T2021. For example, moisture parameters such as ML_MIXR and dew points had correlations between 0.88 - 0.96 with MAEs gradually increasing from low levels (ML_MIXR 0.5 g kg^{-1}) to 500 hPa (dew point 3°C), but with small positive biases (Fig. 2 and Table 2). Parcel parameters, such as ML_LCL, ML_LFC, and ML_CAPE were also well correlated to observations (0.65 - 0.93) with some negative biases and similar magnitude MAEs (< 195 m, < 500 m and 85 J kg^{-1}, respectively) compared to T2021 (Fig. 2 and Table 2). ERA5 appears to underestimate larger ML_CAPE, shown by the locally estimated scatterplot smoothing line (LOESS), also noted by T2021. ML_CIN had a small positive bias (3 J kg^{-1}) and smaller MAE (~15 J kg^{-1}) than T2021.

	Pearson	Spearman	Mean Error (ME)	Mean Absolute Error (MAE)	Root Mean Square Error (RMSE)
Moisture Parameters					
ML MIXR (g kg^{-1})*	0.96	0.96	-0.02	0.56	0.75
10-m dewpoint (°C)	0.95	0.94	0.11	1.62	2.14
850-hPa dewpoint (°C)	0.94	0.94	0.20	1.50	2.30
700-hPa dewpoint (°C)	0.92	0.94	0.10	2.52	3.96
500-hPa dewpoint (°C)	0.88	0.90	0.90	3.21	4.77
Parcel Parameters					
ML CAPE (J kg^{-1})*	0.80	0.74	-33.54	86.59	215.63
ML LI (°C)*	0.97	0.96	0.36	1.09	1.43
ML CIN (J kg^{-1})*	0.61	0.59	3.19	15.98	39.65
ML LCL (m AGL)*	0.93	0.93	-34.01	174.65	238.41
ML LFC (m AGL)*	0.65	0.66	-44.40	504.13	883.75
ML EL (m AGL)*	0.82	0.74	-443.52	1148.91	1839.62
Temperature Parameters					
10-m temperature (°C)	0.96	0.95	-0.43	1.40	1.81
850-hPa temperature (°C)	0.99	0.99	-0.28	0.54	0.77

700-hPa temperature (°C)	0.99	0.99	0.04	0.46	0.65
500-hPa temperature (°C)	0.99	0.99	0.03	0.35	0.53
0-1-km LR (K km^{-1})	0.73	0.68	0.30	1.21	1.65
0-3-km LR (K km^{-1})	0.92	0.91	0.22	0.47	0.62
3-6-km LR (K km^{-1})	0.94	0.93	0.00	0.20	0.26
500-700-hPa LR (K km^{-1})	0.94	0.94	-0.01	0.21	0.28

Table 2: Parcel and thermodynamic parameters statistical error metrics comparing observed and collocated ERA5 profiles. The units for mean error (ME), mean absolute error (MAE), and root-mean-square error (RMSE) are identical to each parameter. The asterisk denotes only unstable environments are considered.

ERA5 temperature parameters had high correlations with observations (all > 0.95) (Fig. 2 and Table 2) with small negative biases (> -0.5°C) and slightly larger MAEs (< 1.5°C) in low levels (10 m to 850 hPa), then improved at 700 and 500 hPa (Table 2). All lapse rates had correlations > 0.9 except for 0 - 1 km (0.73). Small positive biases (~ 0.3 K km^{-1}) only existed in low levels (0-1 km and 0-3 km) (Table 2). Results are similar in magnitude to T2021.

Wind speeds were well correlated with observations, improving with height from 0.74 at 10 m to 0.97 at 500 hPa, with small negative biases (-0.1 to -1.7 m s^{-1}) and MAEs (between 2-3 m s^{-1}) (Fig. 3 and Table 3). ERA5 mean winds were also well correlated to soundings (≥ 0.90), with small biases (0 to -0.2 m s^{-1}) and MAEs (0.6 - 1.1 m s^{-1}) (Fig. 3 and Table 3). Wind shear correlations mimicked wind speeds, with increasing correlations from low levels to higher levels (0.75 - 0.94 m s^{-1}), while biases were between 0.1 to -0.3 m s^{-1} and MAEs all near 2 m s^{-1} (Fig. 3 and Table 3). Finally, ERA5 storm relative helicity (SRH) between 0 - 1 km and 0 - 3 km both showed good correlation to observations (0.82 - 0.85) with relatively small positive biases (~ 5 m^2 s^{-2}) and MAEs (~ 30 m^2 s^{-2}) (Fig. 3 and Table 3). All of the wind parameter errors were similar to those in T2021, but with slightly smaller correlations (0.03 to 0.06 differences) for wind shears.

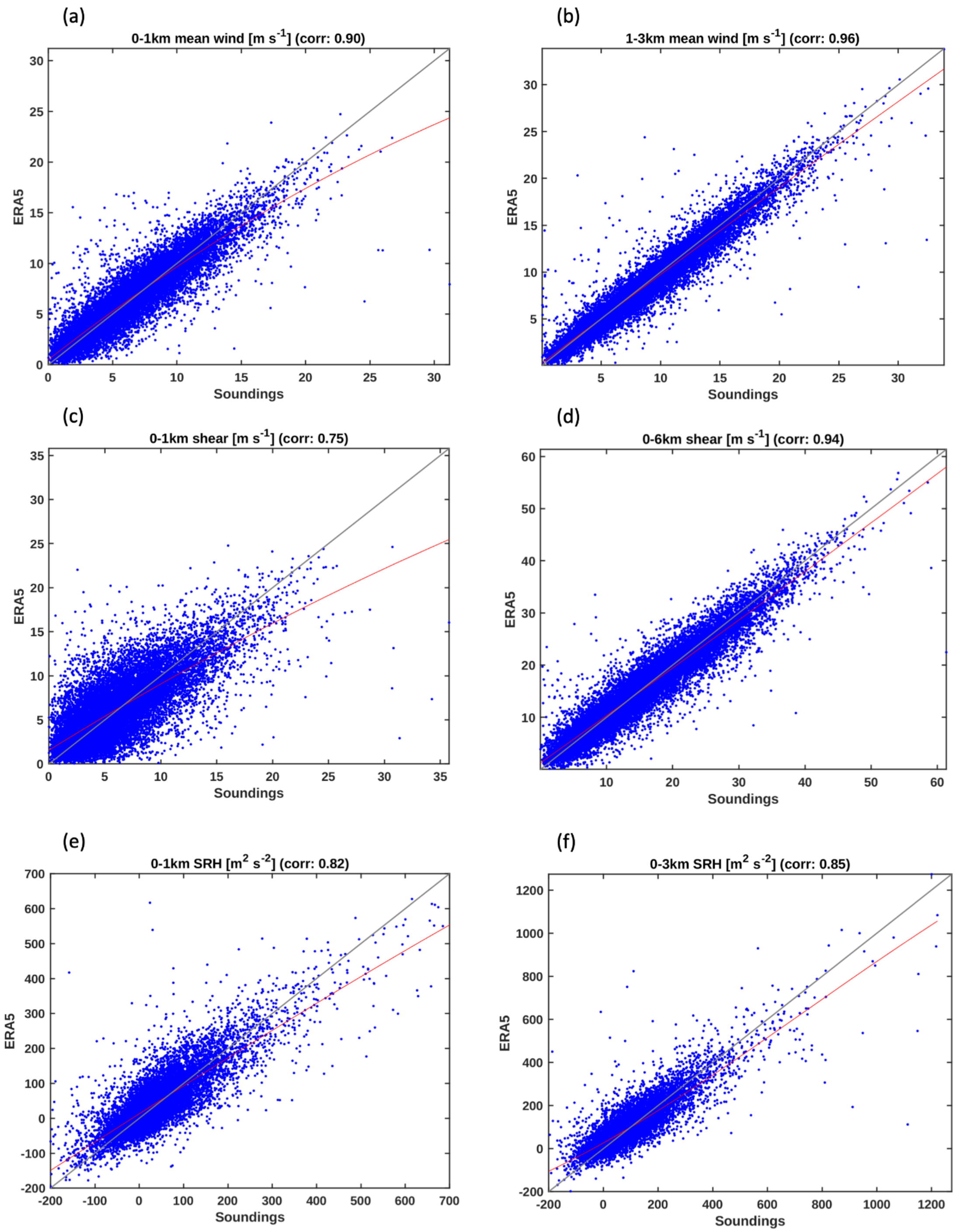

Figure 3: As in Fig. 2 but for (a) 0–1 km mean wind (m s^{-1}), (b) 1–3 km mean wind (m s^{-1}), (c) 0–1 km wind shear (m s^{-1}), (d) 0–6 km wind shear (m s^{-1}), (e) 0–1 km storm relative helicity (SRH; m^2 s^{-2}), and (f) 0–3 km storm relative helicity (SRH; m^2 s^{-2}).

	Pearson	Spearman	Mean Error (ME)	Mean Absolute Error (MAE)	Root Mean Square Error (RMSE)
Wind Parameters					
10-m wind speed (m s^{-1})	0.74	0.73	-1.68	3.28	4.59
850-hPa wind (m s^{-1})	0.91	0.91	-0.07	2.55	3.62
700-hPa wind (m s^{-1})	0.94	0.94	-0.74	2.46	3.49
500-hPa wind (m s^{-1})	0.97	0.97	-0.55	2.37	3.50
0-1-km mean wind (m s^{-1})	0.90	0.90	0.02	1.13	1.60
1-3-km mean wind (m s-1)	0.96	0.96	-0.22	0.88	1.32
0-6-km mean wind (m s^{-1})	0.98	0.98	-0.21	0.64	1.01
Effective shear (m s^{-1})*	0.73	0.66	-0.96	2.74	4.60
0-1-km shear (m s^{-1})	0.75	0.71	0.05	2.02	2.74
0-3-km shear (m s^{-1})	0.86	0.86	-0.31	1.97	2.70
0-6-km shear (m s^{-1})	0.94	0.94	-0.22	2.04	2.81
0-1-km SRH ($m^2 s^{-2}$)	0.82	0.77	5.26	30.81	46.59
0-3-km SRH ($m^2 s^{-2}$)	0.85	0.82	5.13	33.97	54.86
Composite Parameters					
STP*	0.59	0.45	-0.01	0.02	0.16
SCP*	0.68	0.61	-0.13	0.25	0.97
ML WMAXSHEAR*	0.82	0.72	-33.85	76.19	143.22

Table 3: As in Table 2, but for wind and composite parameters. An asterisk indicates that only values > 0 are included in the calculations.

Pointed out by T2021, composite parameters often suffer from the largest error due to the multiplying errors with each term. The more terms in a composite parameter, the larger the error. For example, SCP and STP (both consist of more than two thermodynamic and kinematic terms) had the lowest correlation (0.59-0.68), whereas ML_WMAXSHEAR (consists of only one thermodynamic and one kinematic term) had the highest correlation (0.82) (Fig. 4 and Table 3). However, all of the biases and MAEs are small (Table 3), and smaller than those in T2021. All three ERA5 composite parameters underestimate sounding-derived parameters with increasing magnitude, as shown by the LOESS (Fig. 4).

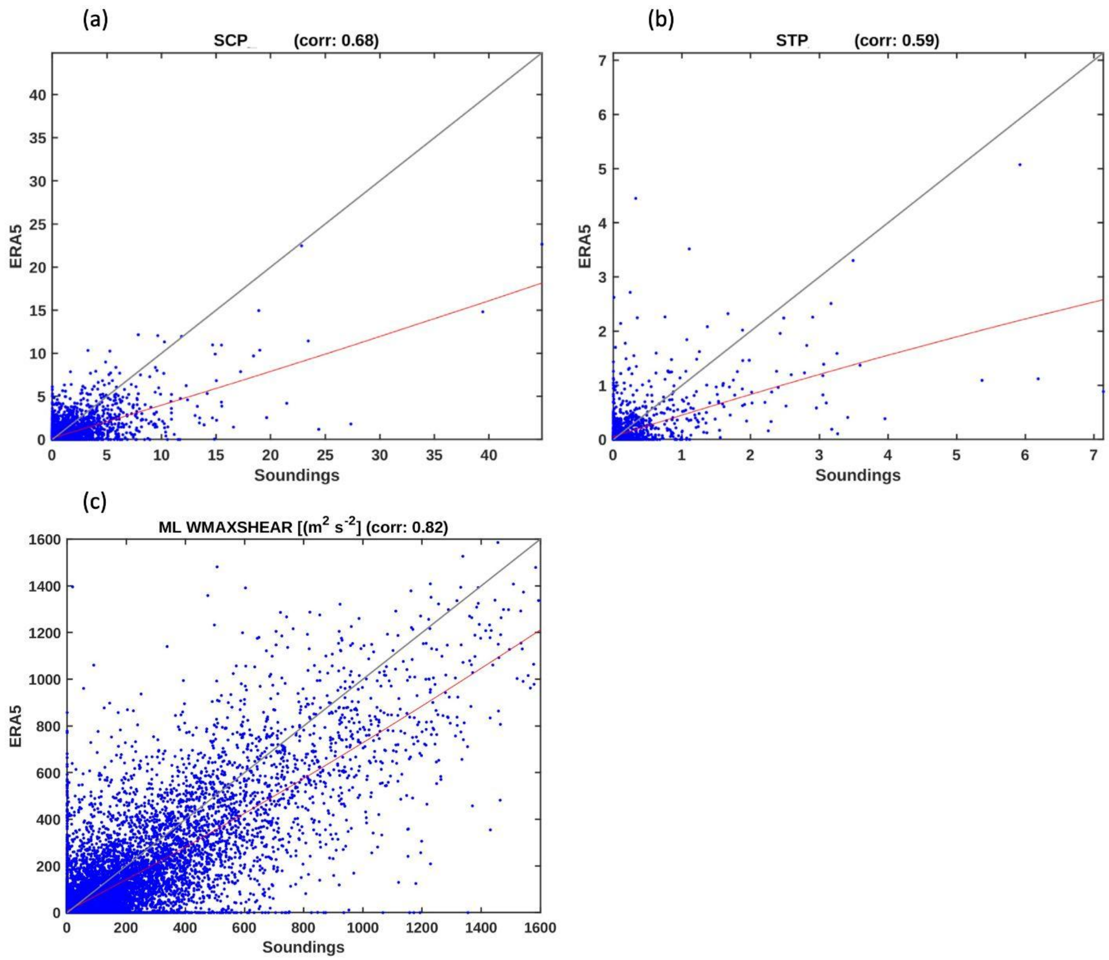

Figure 4: As in Fig. 2 but for (a) supercell composite parameter (SCP; dimensionless), (b) significant tornado parameter (STP; dimensionless), and (c) mixed-layer WMAXSHEAR (m^2 s^{-2}).

2.3 Statistical Analysis for Regional Comparisons

To explore inter-provincial (regionally classified) differences in the convective parameters, univariate tests and visualizations were performed using the package ggstatsplot (Patil 2021) in R (R Core Team 2022). Variables were inspected and the majority were normally distributed although some had heavy-tails and outliers. Given this, rather than non-parametric tests, robust alternatives to the t-test were used: heteroscedastic one-way ANOVAs for trimmed means as the global test (Wilcox 2012), the explanatory measure of effect size (values of ξ =

0.10, 0.30, and 0.50 correspond to small, medium, and large effect sizes; Wilcox and Tian 2011) and Yuen's trimmed means for pairwise post-hoc tests (Yuen 1974). Because of multiple comparisons between regions, p-values for the post-hoc tests were adjusted using the Holm–Bonferroni method (Holm 1979). For the global tests, no adjustments were made to p-values in the ggstatsplots (unadjusted values appear in subtitles), instead, the package candisc (Friendly and Fox 2021) was used to perform a MANOVA using the regionally classified tornado parameters. This approach, unlike the robust methods discussed earlier, accounts for variable interactions in group separation. For the multivariate analysis, the convective parameters were first standardized using the Ordered Quantile Normalization procedure (Peterson and Cavanaugh 2020) and part of the package bestNormalize (Peterson 2021). For Descriptive Discriminant Analysis (DDA) we performed Linear Discriminant Analysis (LDA) in the package candisc, producing a biplot. To examine regional pairwise relationships, and because regional sample size was often smaller than the number of convective parameters, we performed post-hoc comparisons between regions using box-plots created in ggstatsplot from component scores of the significant canonical axes. Yuen's trimmed means was used for pairwise post-hoc tests and p-values were adjusted using the Holm-Bonferroni method. Trends in structure correlations of the convective parameters were examined to typify regional differences in tornado event characteristics.

3. Results

3.1 Thermodynamic Parameters

Only median values will be referenced for regional comparisons throughout the results, since not all regions had normally distributed convective parameters. All related figures in this subsection appear in Fig. 5.

Mixed-layer mixing ratios (ML_MIXR) are highest in S_ON and QC (>14 g kg^{-1}) followed by MB (<14 g kg^{-1}) with N_ON in between (12.5 g kg^{-1}) and decreasing further in SK (11.5 g kg^{-1}) and AB (~10.5 g kg^{-1}) (Fig. 5a). AB and SK are statistically smaller than MB eastward, except for SK versus N_ON. This is not unexpected due to eastern Canada's climate, in contrast to AB, that is in the lee of the Rocky Mountains and void of large inland lakes (e.g. Oke 1998). The AB ML_MIXR is similar to strong AB tornado events based on observed soundings (Dupilka and Reuter 2011). Apart from moisture advection (that likely plays a large role in MB), the Canadian Prairies are reliant on local surface moisture sources, such as annual field crops (e.g. Hanesiak et al. 2004; Brimelow et al. 2011; Hanesiak et al. 2011) that have been linked to its tornado climatology (Raddatz and Cummine 2003). Canadian ML_MIXR magnitudes are within those reported by T2020 for the U.S., with AB being more closely aligned with Europe (T2020) and western U.S. (e.g. Zipser and Golden 1979; Szoke and Weisman 1984).

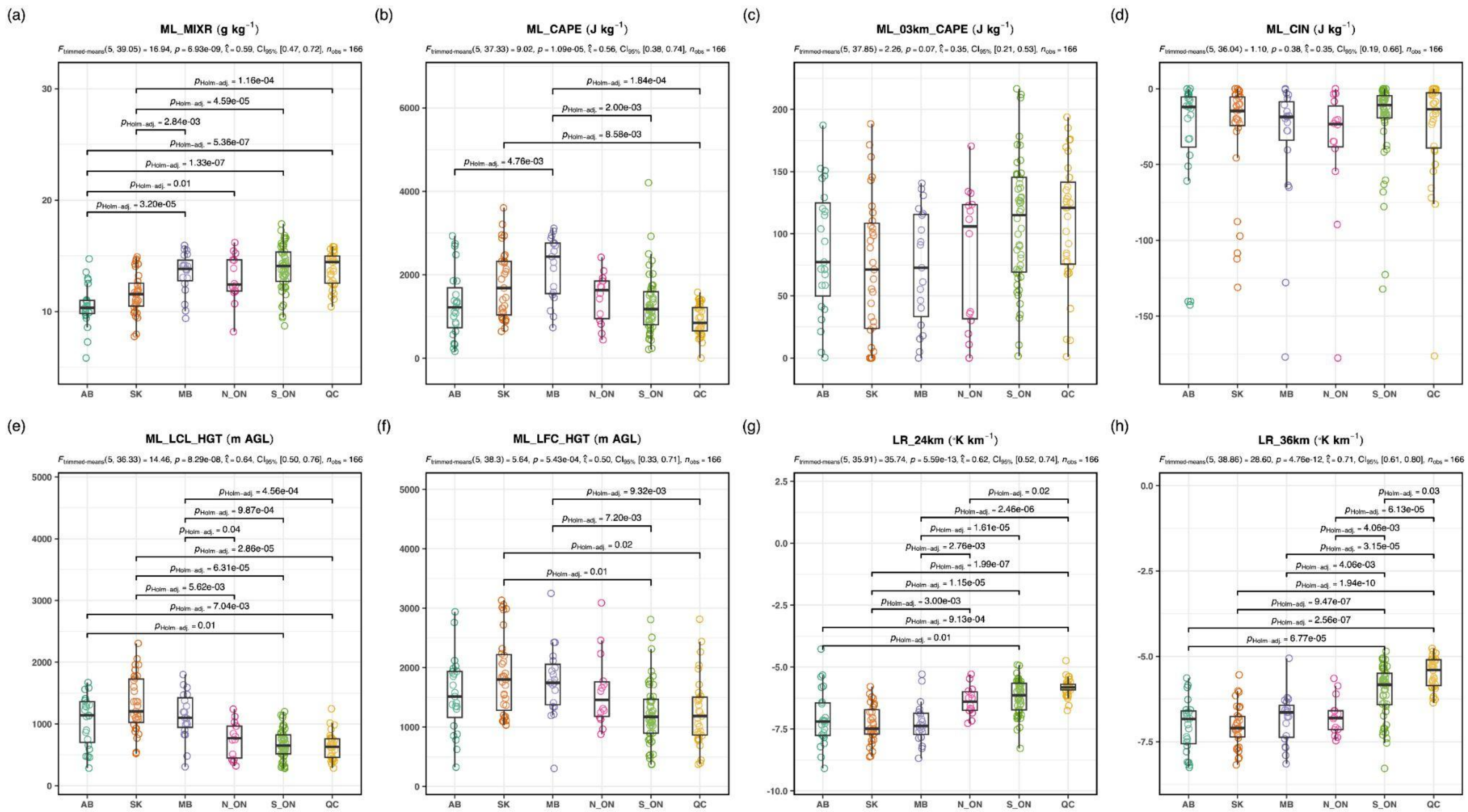

Figure 5: Box-and-whisker plots of (a) ML_MIXR, (b) ML_CAPE, (c) ML_03km_CAPE, (d) ML_CIN, (e) ML_LCL_HGT, (f) ML_LFC_HGT, (g) LR_24km, (h) LR_36km for each Canadian region. The median is the solid horizontal line inside the box, the box edges represent the 25th and 75th percentiles, whiskers represent the 10th and 90th percentiles, and circles are jittered raw data observations. Convective parameter definitions are in Appendix A. Convective variables are calculated from ERA5 proximity grid points.

CAPE is an important parameter linked to updraft intensity, vertical stretching and tornadic supercells (e.g. Fawbush and Miller 1954; Beebe 1958; Maddox 1976; Brooks et al. 1994; Thompson et al. 2003, 2004). ML_CAPE displays a bell-type curve with respect to regional median differences, with MB highest (> 2400 J kg^{-1}), SK and N_ON near 1700 J kg^{-1}, AB and S_ON near 1200 J kg^{-1}, while QC is lowest (~ 900 J kg^{-1}) (Fig. 5b); SK is statistically higher than QC, and MB is statistically higher than AB, S_ON and QC. Low level moisture is not the only factor that determines strong tornado CAPE environments since the regional patterns of ML_MIXR and ML_CAPE are dissimilar. ML_CAPE are slightly higher than T2020, and may be due to (a) T2020 combining all U.S. data, (b) a lack of nocturnal events in this study, and/or (c) filtering of tornado cases to minimize environment oversampling. However, Grams et al. (2012) showed that U.S. northern plains significant tornado events are typically associated with higher ML_CAPE (median ~ 2100 ± 900 J kg^{-1}) compared to other U.S. regions; SK/MB/N_ON would fall into northern plains and Chinese (Zhang et al. 2023) environments. In contrast, S_ON/QC ML_CAPE are aligned with U.S. midwest environments. AB ML_CAPE is comparable to AB $F2^+$ events in Dupilka and Reuter (2006a) as well as Colorado case studies (e.g. Murdzek et al. 2020).

Rasmussen (2003) found that 0 - 3 km CAPE may be important for enhancing low level updrafts and vertical stretching in U.S. tornadic supercells; median was ~70 J kg^{-1}. S_ON and QC have the largest ML_03km_CAPE (115-120 J kg^{-1}), with N_ON second (105 J kg^{-1}) and AB/SK/MB all being similar (70 -75 J kg^{-1}) (Fig. 5c); differences are not statistically significant mainly due to variability, however, S_ON/QC had a greater number of larger magnitude cases (dots in Fig. 5c). All magnitudes are within Rasmussen's U.S. and T2020 U.S. and European thresholds, but on the upper end in S_ON/QC.

Convective inhibition is critical to assess convection initiation likelihood, but also important for the build up of energy to produce explosive (tornadic) storms (e.g. Fawbush and Miller 1954; Beebe 1955, 1958; Maddox 1976). MB/N_ON have the most negative ML_CIN (~ -20 J kg^{-1}), while AB/S_ON/QC have the least negative (-10 to -13 J kg^{-1}), and SK is in between (-15 J kg^{-1}) (Fig. 5d); none are statistically different due to large variability. However, using the medians at face value, comparisons to T2020, Brooks et al. (1994), Davies (2004) and Zhang et al. (2023) suggests that central North American environments may have higher convective inhibition compared to western and eastern counterparts, but similar to China.

Low ML_LCLs have been linked to tornadic storms by lowering the mid level updraft and increasing vertical stretching (e.g. Rasmussen and Blanchard 1998; Edwards and Thompson 2000; Thompson et al. 2003). ML_LCL are highest in SK (1200 m) with MB/AB being very close (1100 m), 775 m in N_ON, while S_ON/QC have the lowest (630 - 650 m) (Fig. 5e); AB is statistically higher than S_ON/QC, while SK/MB are statistically higher than N_ON/S_ON/QC. Similarly, SK and MB have the highest ML_LFC (1750 - 1800 m), with AB/N_ON near 1450 - 1500 m, and S_ON/QC the lowest (~ 1180 m) (Fig. 5f); SK/MB are statistically higher than S_ON/QC. Eastern regions have the lowest LCLs and LFCs primarily due to more abundant boundary layer moisture and smaller dew point spreads (discussed in Section 3.5). LCLs and LFCs in eastern Canada are near typical U.S. and European heights (e.g. Brooks et al. 1994; Davies 2004; T2020; Rodríguez and Beach 2020; Pilguj et al. 2021), N_ON similar to China (Zhang et al. 2023), while western Canada is higher and similar to U.S. northern plains (e.g. Thompson et al. 2003; Davies 2004). AB is similar to Dupilka and Reuter (2011).

Lapse rates are intrinsically linked to associated CAPE, and they all suggested similar trends. LR_03km was largest in AB/SK/MB (near -7.5 K km^{-1}), while N_ON/S_ON/QC were all between -6 to -6.5 K km^{-1} (not shown); western regions were all statistically more negative than eastern regions. LR_24km was largest in SK/MB (near -7.5 K km^{-1}), then AB (> -7 K km^{-1}), followed by N_ON/S_ON (-6 to -6.5 K km^{-1}), and QC (> -6 K km^{-1}) (Fig. 5f); western regions were statistically more negative than eastern regions, except AB versus N_ON, and N_ON was statistically more negative than QC. LR_36km in AB/SK/MB/N_ON were near -7 K km^{-1}, with S_ON > -6 K km^{-1} and QC > -5.5 K km^{-1} (Fig 5g); all regions west of QC (and S_ON) were statistically more negative. In general, western Canada has 1-1.5 K km^{-1} steeper lapse rates than eastern regions; this in combination with regional ML_MIXR patterns may contribute to the regional pattern in ML_CAPE. Overall, eastern Canada has similar lapse rates as U.S., European and most Chinese counterparts (e.g. Johns and Doswell 1992; Rasmussen and Blanchard 1998; T2020; Zhang et al. 2023).

3.2 Kinematic Parameters

Several mean wind layers were examined, all showing similar increasing trends from western to eastern Canada. For MW_01km (MW_06km), AB/SK/MB were between 7 - 9 m s^{-1} (11 – 14 m s^{-1}), N_ON 11 m s^{-1} (17 m s^{-1}), while S_ON/QC were largest between 12-13 m s^{-1} (19

- 21 m s^{-1}) (not shown); AB/SK (MB/N_ON) are statistically different than the three eastern regions (QC) for MW_01km, while western regions (N_ON) are statistically different than all three eastern regions (QC). Western (eastern) Canada magnitudes are smaller than (as large as) many U.S. strong tornado environments (e.g. Darkow 1969; Kerr and Darkow 1996; Markowski et al. 2003). The MW_13km was used as a surrogate for the low level jet (LLJ) in T2020, and analysis revealed that QC was highest (22 m s^{-1}), S_ON 19 m s^{-1}, N_ON 17 m s^{-1}, and AB/SK/MB 10 – 12 m s^{-1} (Fig. 6a); western areas were statistically smaller than S_ON/QC (including N_ON versus AB/SK) as well as N_ON versus QC. The LLJ winds in western Canada are on the low end of European events, while eastern Canada are comparable to upper-end and median events in Europe and U.S., respectively (compared to Markowski et al. 2003 and T2020).

Wind shear is critical for convection organization, storm rotation and longevity (e.g. Johns and Doswell 1992; Johns et al. 1993; Markowski et al. 1998; Rasmussen and Blanchard 1998; Markowski et al. 2003; Thompson et al. 2003). Bulk wind shears generally increased from west to east in Canada. Between 0 - 1 km (BS_01km), N_ON/S_ON (12 m s^{-1}) is twice as large as (and statistically different than) AB/SK/MB (near 6 m s^{-1}), with QC having the largest values (16 m s^{-1}) and statistically different than any other region (Fig. 6b). BS_03km and BS_06km show similar trends (Fig. 6c,d) but with N_ON becoming similar to the west with height, while effective bulk shear (BS_EFF) has less range between west and east; AB 15 m s^{-1}, SK/MB/N_ON 18 - 19 m s^{-1}, S_ON 23 m s^{-1}, and QC with the highest near 25 m s^{-1} (Fig. 6e). For BS_03km, western regions (N_ON) are statistically different from S_ON/QC (QC), QC is statistically larger than western regions for BS_06km, AB (SK/MB) is statistically different from S_ON/QC (QC) for BS_EFF. Where comparisons were possible, results suggest western (eastern) Canada wind shears are smaller than (as large as) typical U.S. and European strong tornado environments (e.g. Thompson et al. 2003; Markowski et al. 2003; T2020; Rodríguez and Beach 2020; Pilguj et al. 2021). China and western Canada have similar wind shear magnitudes (Zhang et al. 2023).

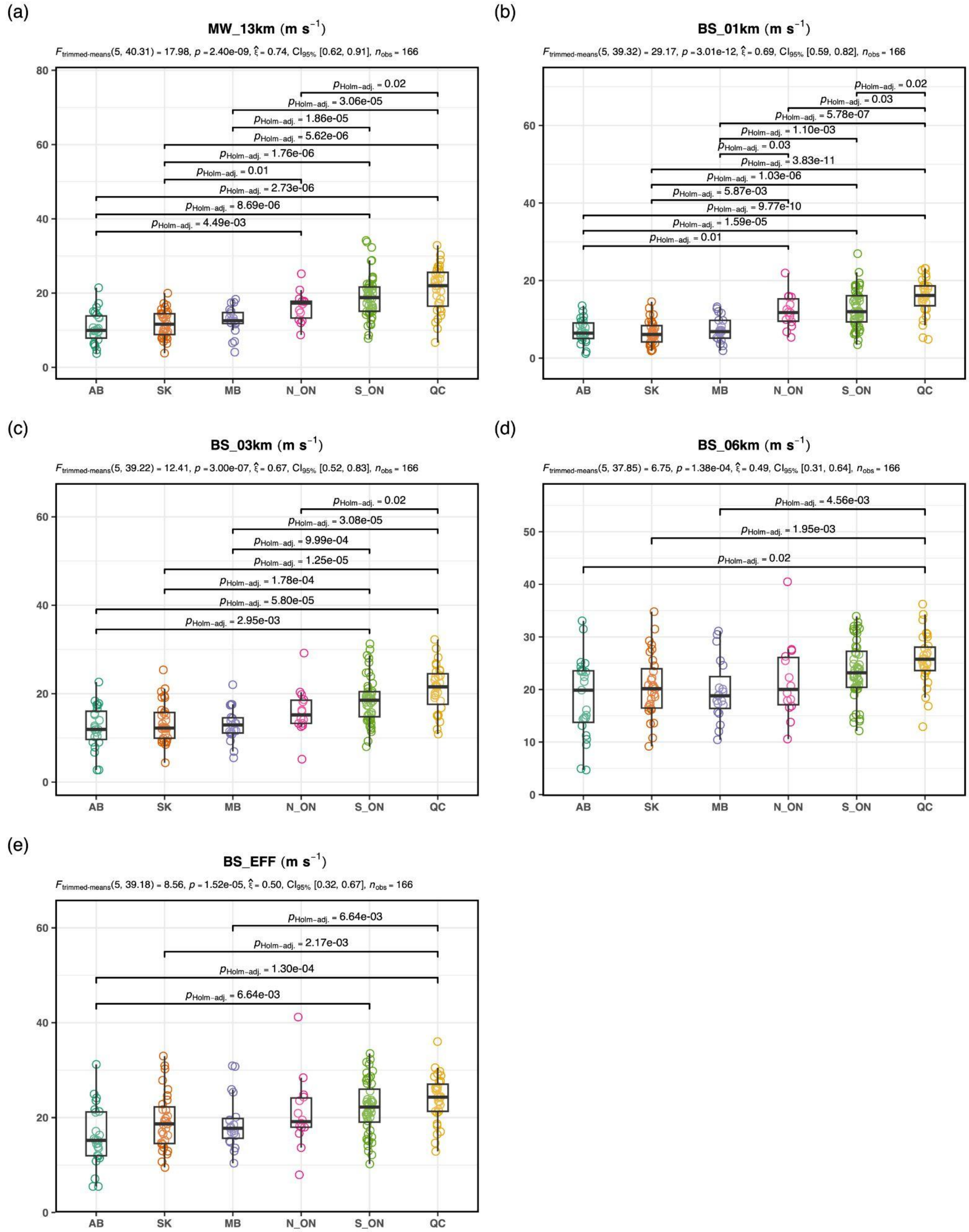

Figure 6: As in Fig. 5, but for (a) MW_13km, (b) BS_01km, (c) BS_03km, (d) BS_06km, (e) BS_EFF.

Storm relative helicity (SRH) has been used to distinguish tornadic versus non-tornadic storms, with higher magnitudes linked to stronger tornadoes (e.g. Davies-Jones 1984; Davies-Jones et al. 1990; Markowski et al. 2003; Thompson et al. 2003). SRH (for right moving storms) increases from west to east in Canada, with SRH_100m_RM varying from 18 - 22 $m^2 s^{-2}$ in AB/SK/MB, 55 $m^2 s^{-2}$ in N_ON and 65 - 80 $m^2 s^{-2}$ in S_ON/QC. SRH_500m_RM ranges between 40 - 55 $m^2 s^{-2}$ in AB/SK/MB, >100 $m^2 s^{-2}$ in N_ON, 150 $m^2 s^{-2}$ in S_ON, and near 170 $m^2 s^{-2}$ in QC (Fig. 7a,b). The 0 - 100 m and 0 - 500 m layers were included since Coffer et al. (2019, 2020) showed they were the most skillful SRH parameters in predicting strong tornadic supercells, however, their median magnitudes (>80 $m^2 s^{-2}$ for 0 - 100 m; >200 $m^2 s^{-2}$ for 0 - 500 m) were higher than Canadian cases. They also noted that these lowest layers have better forecast skill in the south and eastern U.S. compared to the northern plains. SRH_1km_RM ranged between 70 to 90 $m^2 s^{-2}$ in AB/SK/MB, 130 $m^2 s^{-2}$ in N_ON, 180 $m^2 s^{-2}$ in S_ON, and 230 $m^2 s^{-2}$ in QC, while SRH_3km_RM were between 130 $m^2 s^{-2}$ in AB to 180 $m^2 s^{-2}$ in MB/N_ON, with S_ON and QC being the highest (225 $m^2 s^{-2}$ and 300 $m^2 s^{-2}$, respectively) (Fig. 7c,d). In general, western regions are statistically smaller than eastern regions for all SRH layers. AB SRH_1km_RM (SRH_3km_RM) are slightly larger (smaller) compared to Dupilka and Reuter (2011), however, this could be due to different datasets as well as sample sizes. Western Canada SRH_1km_RM are smaller than the U.S. and most Chinese counterparts, however, from MB eastward, SRH_3km_RM are similar to U.S., European and Chinese magnitudes (compared to Thompson et al. 2003; Coffer et al. 2020; T2020; Zhang et al. 2023).

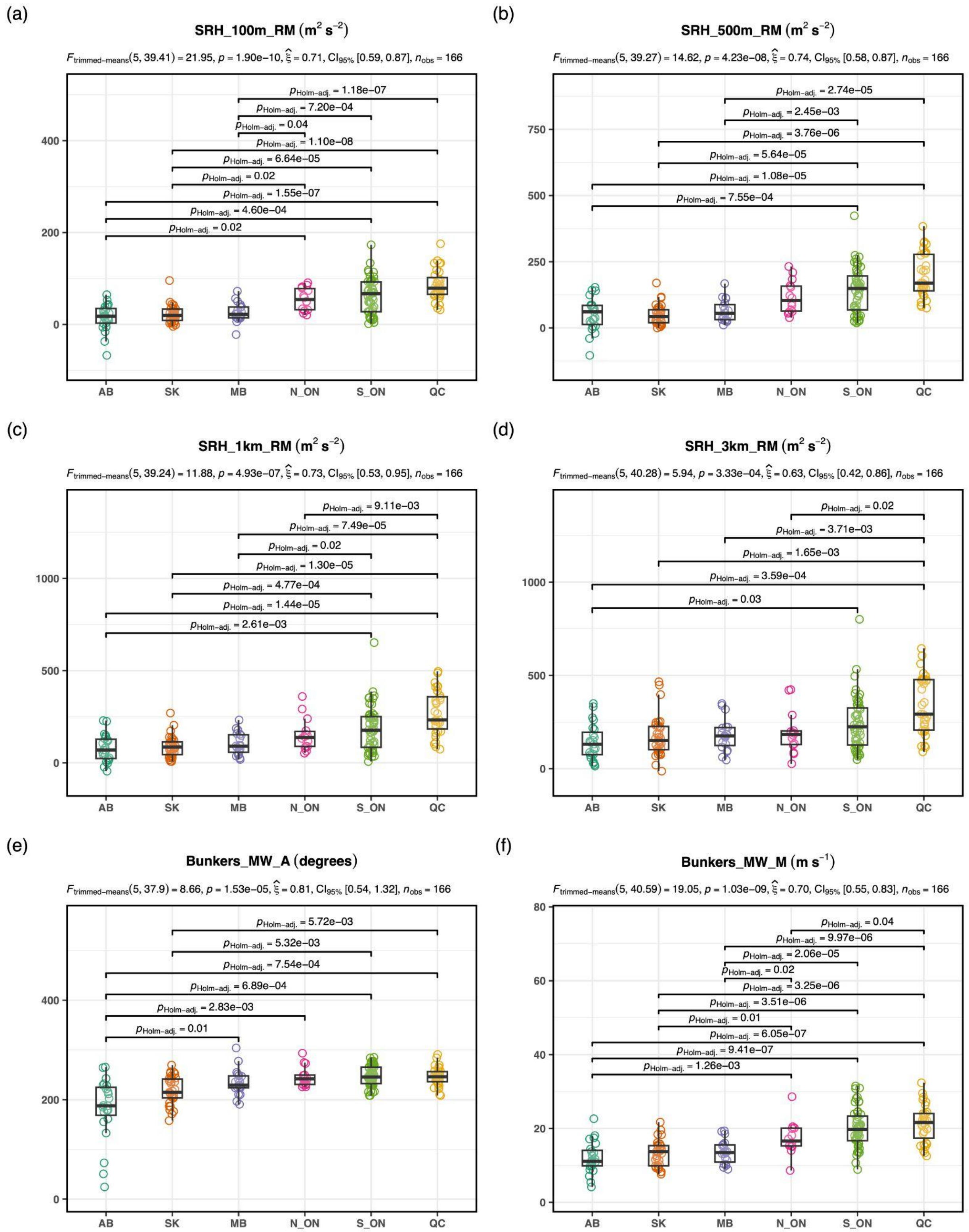

Figure 7: As in Fig. 5, but for (a) SRH_100m_RM, (b) SRH_500m_RM, (c) SRH_1km_RM, (d) SRH_3km_RM, (e) Bunkers_MW_A, and (f) Bunkers_MW_M.

Bunkers et al. (2000) storm motions were used to reveal mean (normal) storm tracks and right-deviant storm motions, since there has been no formal climatology of tornadic storm motions in Canada. However, it should be noted that this technique has biases, particularly for significantly tornadic supercells (Bunkers 2018). Mean (normal) storm motion (Bunkers_MW_A) shifts from SSW in AB to WSW once in N_ON/S_ON/QC (Fig. 7e) and increase in mean speed (Bunkers_MW_M) from 12 m s^{-1} in AB, 14 m s^{-1} in SK/MB, 16 m s^{-1} in N_ON, and 19 - 22 m s^{-1} in S_ON/QC (Fig. 7f); AB (SK) is statistically different from MB eastward (S_ON/QC) for mean storm track direction, while all western regions (N_ON) are statistically different from all eastern regions (QC) for mean storm velocity. Dupilka and Reuter (2011) showed that AB tornadic storms track from ~250° at 13 m s^{-1}; results here have a more southerly component, but velocity is similar. Right-moving storms (Bunkers_RM_A) track from 220° in AB (statistically different than all eastern areas), 250° in SK and westerly elsewhere, with speeds near 10 - 11 m s^{-1} in AB/SK/MB (statistically different from eastern regions), 16 m s^{-1} in N_ON, and 18 - 19 m s^{-1} in S_ON/QC (not shown). This suggests that the most right-deviant storms (R_Mover_Dev) occur in MB (43°) (statistically different from S_ON/QC), followed by SK/AB (36 - 39°) (statistically different from all eastern regions), with N_ON/S_ON/QC very similar (22 - 24°) (Fig. 8a). Based on the authors' experience, the mean and right-deviant Bunkers storm track directions are reasonable, although individual storms/cases can be different.

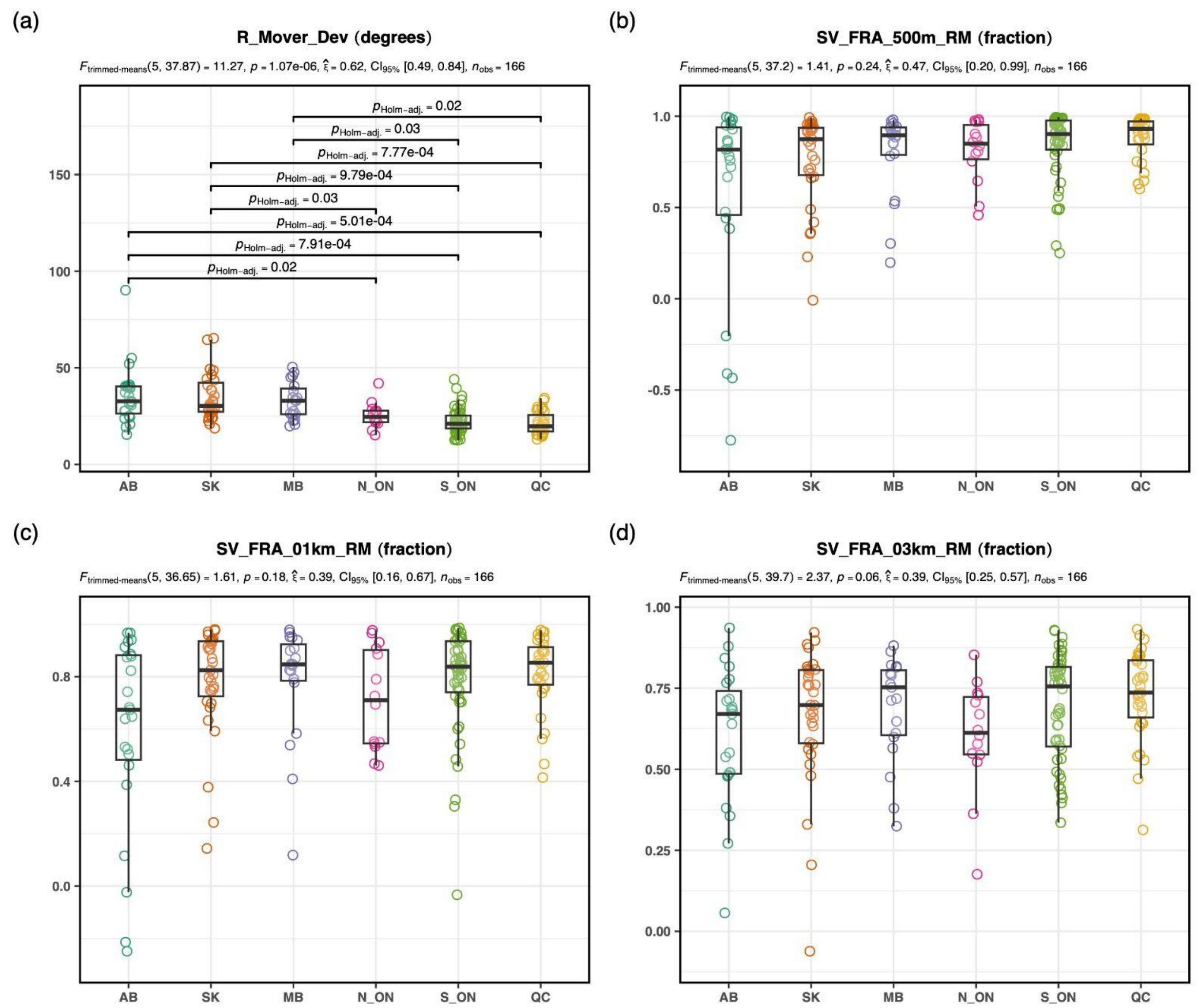

Figure 8: As in Fig. 5, but for (a) Bunkers right-mover deviation (R_Mover_Dev), (b) SV_FRA_500m_RM, (c) SV_FRA_01km_RM, (d) SV_FRA_03km_RM.

Finally, higher streamwise vorticity fraction has been linked to longer-lived supercells and tornado occurrence likelihood (e.g. Davies-Jones 1984; Rutunno and Klemp 1985; Markowski et al. 2003; Orf et al. 2017; Peters et al. 2023). However, Coffer et al. (2019) suggests that low level SRH (e.g. SRH ≤ 500 m AGL) is just as good as any measure of streamwise vorticity. MB/S_ON/QC have the highest streamwise vorticity fraction (>90 %), particularly between 0 - 500 m (SV_FRA_500m_RM) compared to other regions (82 - 87%), especially AB (Fig. 8b); QC has much less variability compared to other regions. Although streamwise vorticity fraction differences between regions are smaller for 0 - 1 km (SV_FRA_01km_RM) and 0 - 3 km (SV_FRA_03km_RM), AB still stands out to be smaller than other regions (Fig. 8c, d). N_ON also has smaller fractions, however, it is not clear if this is partially due to sample sizes. Although the regional streamwise vorticity differences may be meteorologically important, none are statistically significant. Significant U.S. tornado streamwise vorticity magnitudes in Markowski et al. (2003) (> 0.01 s^{-1}) were similar to eastern Canada, but nearly twice as large as western Canada (not shown).

3.3 Composite and Other Indices

Other indices that showed west-east differences included the Moisture_Flux_02km (g s^{-1} m^{-2}) and Cold_Pool_Strength (K); see Appendix A for definitions. The moisture flux between 0 - 2 km signifies horizontal moisture flows that are critical for supplying storm energy, while the cold pool strength has been linked to tornadic versus non-tornadic supercells (e.g. Markowski et al. 2002). Large increases in Moisture_Flux_02km from west to east are noted, from AB (60 g s^{-1} m^{-2}), SK (75 g s^{-1} m^{-2}), MB/N_ON (110 - 115 g s^{-1} m^{-2}) with highest levels in S_ON/QC (180 - 200 g s^{-1} m^{-2}) (Fig. 9a); AB is statistically different from MB eastward and, SK/MB (N_ON) is statistically different from S_ON/QC (QC). Based on the authors' experience, and results herein (i.e. ML_MIXR and mean low level winds), these regional differences are not surprising since eastern Canada is a more humid climate (e.g. Oke et al. 1998). Larger cold pool strengths can lead to tornadogenesis failure (Markowski et al. 2002), and results suggest that western regions have significant tornadoes despite having colder cold pools (predicted by the method used here); cold pool strength was highest in SK/MB (>12 K) and statistically different from all eastern regions, then AB (10 K) that is statistically different from MB/QC, with eastern regions (N_ON/S_ON/QC) being the smallest (7 - 7.5 K) (Fig. 9b).

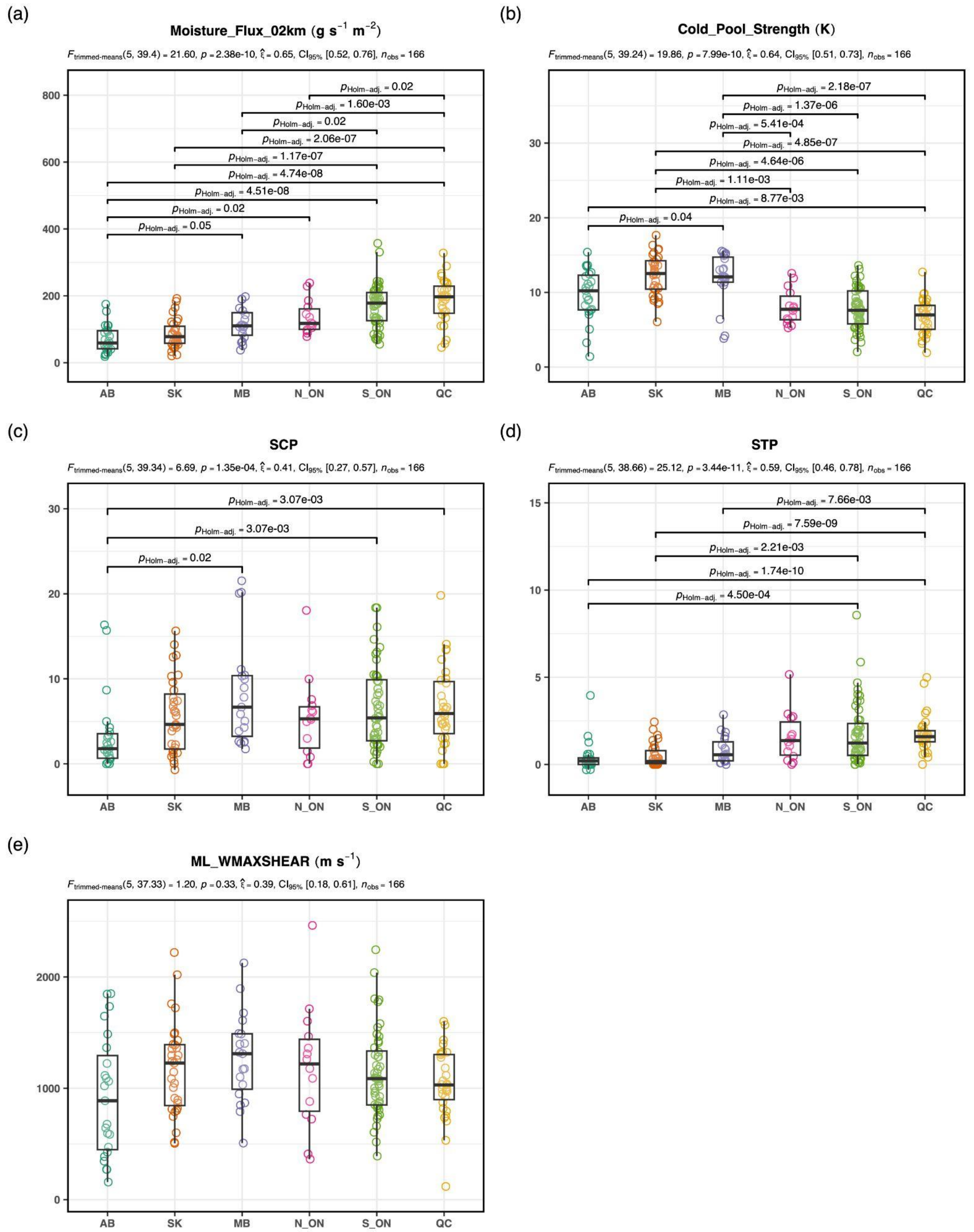

Figure 9: As in Fig. 5, but for the (a) Moisture_Flux_02km, (b) Cold_Pool_Strength, (c) SCP, (d) STP, and (e) ML_WMAXSHEAR.

Common parameters for strong tornadic storms include the supercell composite parameter (SCP) and significant tornado parameter (STP); see Appendix A (e.g. Thompson et al. 2003, 2004, 2007; Gropp and Davenport 2018; Coffer et al. 2019). Only SCP from Gropp and Davenport (2018) and STP from Coffer et al. (2019) will be discussed, since trends are similar to older SCP and STP formulations. SCP increases from AB (1.8) to SK (4.6), peaking in MB (6.8), then remains 5.3 - 5.9 eastward; only AB versus MB/S_ON/QC were statistically different (Fig. 9c). The western Prairies are similar to typical northern plains and European values (e.g. Grams et al. 2012; T2020), while MB eastward are smaller than tornadic supercells in Thompson et al. (2003) but similar to China (Zhang et al. 2023) and general supercells in Thompson et al. (2004). STP increases markedly from western to eastern Canada with AB/SK near 0.20 (statistically different from S_ON/QC), MB 0.5 (statistically different from QC), and N_ON/S_ON/QC between 1.3 - 1.6 (Fig. 9d). Western provinces are similar to European magnitudes (T2020) and within the bottom end of U.S. northern plains (Grams et al. 2012) and China (Zhang et al. 2023). Eastern Canada is near lower-end values of Thompson et al. (2004) and the midwest U.S. and Chinese medians (Grams et al. 2012; Zhang et al. 2023). Overall, the STP, and possibly SCP, would have to be recalibrated for Canada, particularly in western Canada.

ML_WMAXSHEAR ($m^2\ s^{-2}$) has been found to be useful for identifying severe storm environments that combine maximum theoretical updraft speed and 0 - 6 km bulk wind shear in both Europe and U.S. (Brooks 2013; Taszarek et al. 2017; T2020); see Appendix A. SK/MB/_N_ON have the highest magnitudes (1200 - 1300 $m^2\ s^{-2}$), with S_ON/QC near 1000 $m^2\ s^{-2}$, and AB is lowest (~875 $m^2\ s^{-2}$) (Fig. 9e). None are statistically different. AB is within common F0-F1 European and low-end F2/F3 U.S. magnitudes, while S_ON/QC is near U.S. EF2/3 scales and SK/MB/N_ON are within all U.S. tornado EF-scales (when compared with T2020).

3.4 Regional Discrimination of Combined Parameters

To put regional comparisons from Sections 3.1-3.3 into perspective, and to determine overall regional significance, MANOVA and LDA were performed, the former providing statistical tests and latter providing a biplot for interpretation (Fig. 10a-c). Unlike the univariate methods presented previously, these approaches include possible variable interactions that further discriminate among geographic regions. Family-wise error rate is also controlled as the method extracts composite discriminant axes that can be tested for group separation. The first two canonical discriminant axes were most significant (Wilk's Λ=0.05, p-value < $2.2e^{-16}$ and Λ=0.32, p-value = $1.6e^{-04}$, respectively), with additional multivariate statistics provided in the subtitles for Fig. 10a-b. The third and subsequent discriminant axes (not shown) were not significant.

The convective parameters differ significantly amongst all regions in Canada as evidenced by pairwise tests (Fig. 10a-b) and non-overlapping confidence intervals (95% Fig. 10c). The first discriminant axis (78.7% canonical discrimination) associated with the partitioning western to eastern Canada sites, indicates that the most significant differences in convective parameters follow a west to east gradient. On the first axis, all pairwise post-hoc comparisons between regions are significant, with the exception of AB versus SK and S_ON versus QC (Fig. 10a,c). There is significant but comparatively lesser separation (9.4% canonical discrimination) between the prairie provinces and between the eastern provinces (S_ON and QC) on the second axis, however, both AB versus SK and S_ON versus QC were significantly different (Fig. 10b-c). The comparisons for Fig. 10a-b used univariate pairwise tests based on Yuen's trimmed means applied to the axes scores (pooled by region). Ideally, a pairwise multivariate test such as Hotelling's T^2 test would be performed, but the number of parameters examined here exceed the group-wise sample sizes. That the constructed discriminant axes are significant using these tests, without the benefit of variable interactions, is instructive.

The convective parameters ML_LCL_HGT, R_Mover_Dev, Cold_Pool_Strength, ML_LFC_HGT, and ML_CAPE exhibit the most negative structural correlations on the first axis ranging from -0.64 to -0.34, and trend with the Prairie Provinces (Fig. 10c). Conversely, all other convective parameters have positive structure correlations on the first axis and are associated with S_ON/QC. In the top five, BS_01km has the largest structure correlation (0.69) with Bunkers_MW_M, MW_13km, SRH_100m_RM, SRH_500m_RM having correlations >0.68 (Fig. 10c); these are all wind-related parameters. On the second axis, the largest positive structure correlation was LR_24km (0.19) but the highest absolute (negative) correlation was ML_CAPE (-0.55) followed by ML_MIXR, Bunkers_MW_A, ML_WMAXSHEAR, and SCP; most significant parameters are thermodynamic-related.

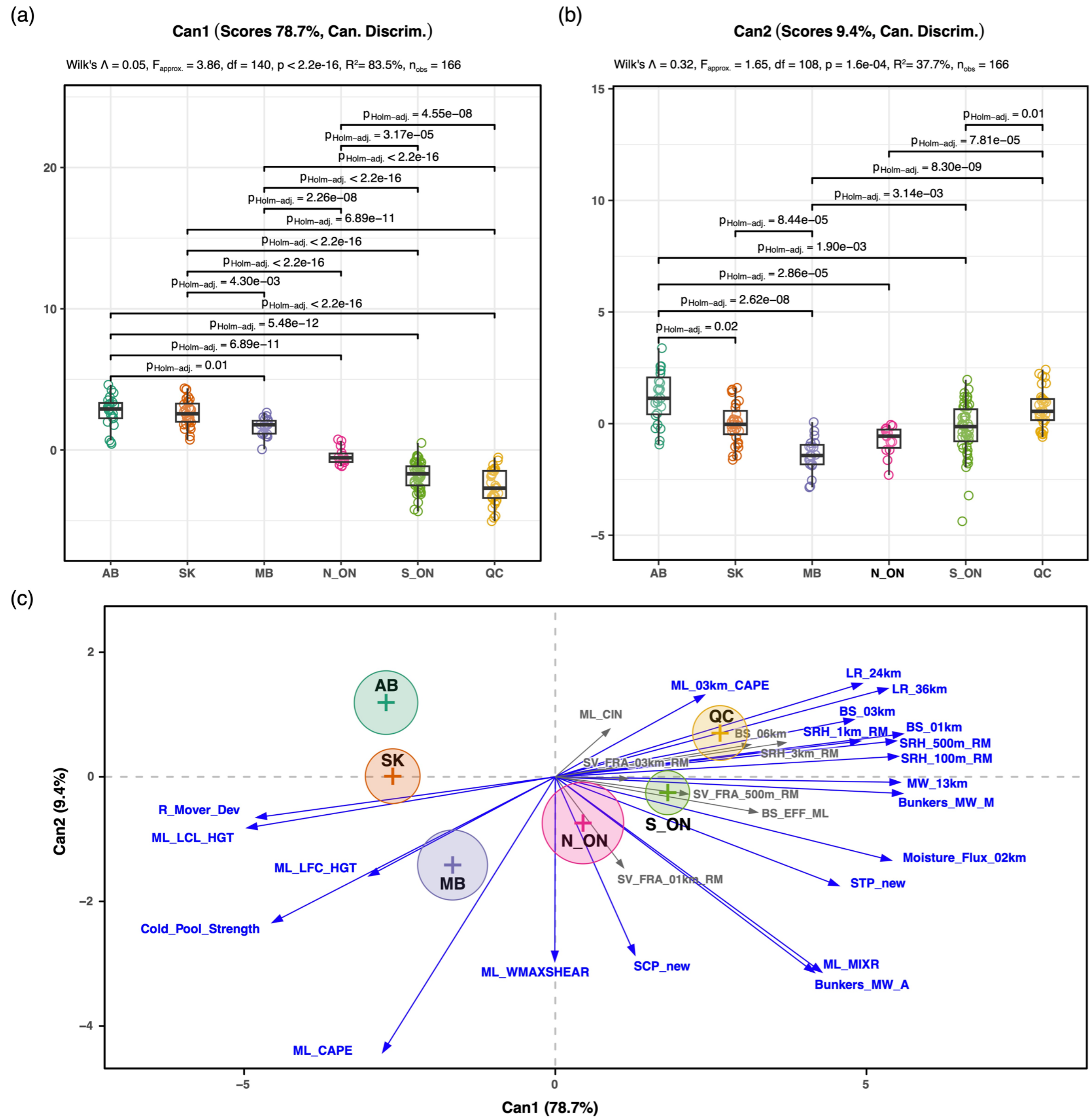

Figure 10: Summary of the canonical discrimination of all of the ERA5-derived convective parameters described in this paper. (a) canonical axis 1 regional boxplots based on axis scores with post-hoc comparisons, (b) as with (a) but for canonical axis 2. Axes are unitless discriminant scores, with percentage of discrimination, and overall axis significance. (c) LDA biplot with regional means, 95% confidence intervals (circles), and structure correlations of the convective parameters with the canonical axes.

3.5 Composite Skew-T's and Hodographs

Composite skew-t and hodographs were generated from the raw ERA5 vertical profiles in each region (Fig. 11 and 12). The "averaging" scheme for the skew-t's stems from Warren et al. (2021) who used a vertical profile of relative humidity and parcel buoyancy for averaging.

The SK/MB skew-t's reveal classic "loaded gun" soundings with larger capping inversions and ML_CAPE, compared to other regions (Fig. 11 and Fig. 5). However, the boundary layer is deeper and drier (i.e. larger dew point spreads) in SK/MB compared to eastern regions, leading to higher LCLs and LFCs (Fig. 11 and Fig. 5), which also creates higher convective temperatures in SK/MB (>30°C) compared to S_ON/QC (~ 26-27°C). Interestingly, mixed-layer parcel convective cloud depths (ML_EL_HGT minus ML_LFC_HGT) are largest in S_ON/QC and smallest in AB, while eastern regions (particularly S_ON/QC) have skinnier ML_CAPE compared to SK/MB (Fig. 11); although theoretical equilibrium levels (EL) are similar between SK/MB/S_ON/QC (11.2 - 12.0 km), prairie ML_LFCs are higher, leading to shallower total convective cloud depth (see also Fig. 5). This is also related to S_ON/QC having larger ML_03km_CAPE than any other region. S_ON/QC also have smaller dew point spreads above the boundary layer compared to Canadian Prairies, that can lead to less dilution of convective updrafts (e.g. Houston and Niyogi 2007) and warmer cold pools (Markowski et al. 2002); however, S_ON/QC have less steep lapse rates (Fig. 5) that can counter reduced dilution (Houston and Niyogi 2007). Chinese composite skew-t's are most similar to eastern Canada.

Composite hodographs (Fig. 12) reveal that western regions (particularly AB) have significantly more 0 - 1 km curvature and less bulk shear, that partially explains why streamwise vorticity is higher in eastern regions (seen in Fig. 7), and suggests that western regions have more of a directional and speed shear mix compared to eastern regions that have large speed shears and SRH in low levels (see Figs. 6 and 7). The shape and low level curvature in the AB hodograph is similar to Dupilka and Reuter (2011) and may be related to mountain-plains processes (Strong 1986), while it appears that MB and China have the most similar hodographs. Visual evidence of larger wind speeds and shears between 0 - 1 km (and above) in eastern Canada can be seen (Fig. 12). Interestingly, eastern Canada experiences larger upper tropospheric (6 - 12 km) winds (shown by the wind barbs beside the skew-t's) that can lead to differences in storm speed, supercell type, and updraft width that can assist with higher mass fluxes to promote more precipitation and affect downdraft characteristics (e.g. Rasmussen and Straka 1998; Warren et al. 2017). However, storm type and morphology are beyond the scope of this study.

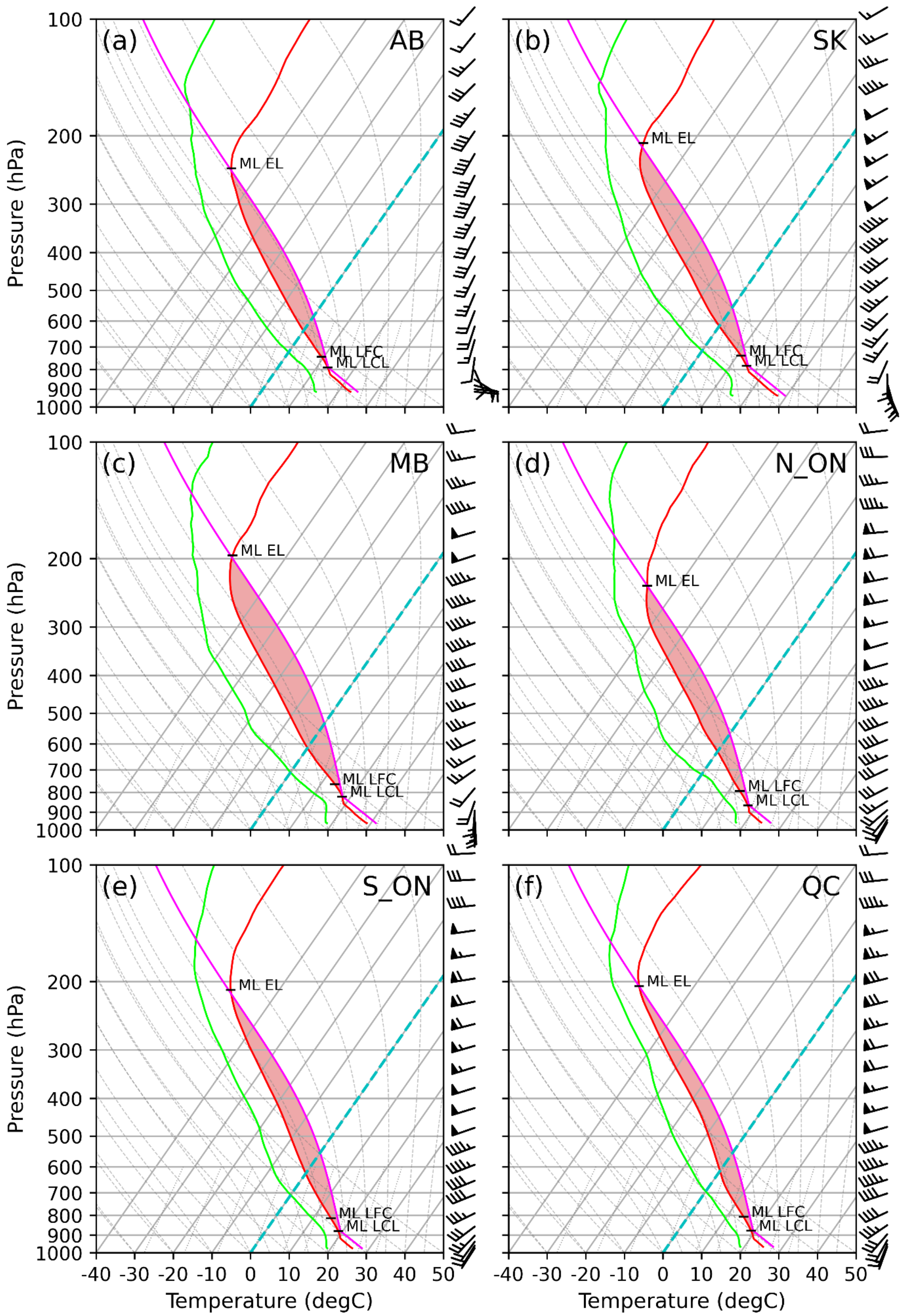

Figure 11: Composite skew-t's for each of the 6 regions using 0-500 m mixed layer: (a) AB, (b) SK, (c) MB, (d) N_ON, (e) S_ON, and (f) QC. The averaging technique is explained in the text. Wind barbs in knots.

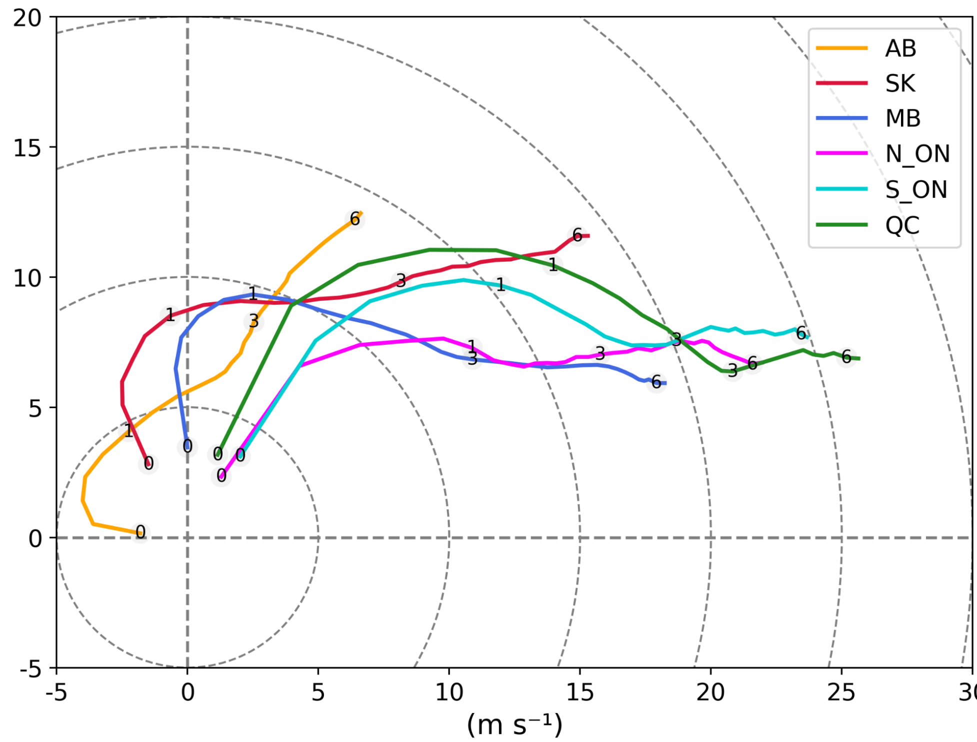

Figure 12: Composite hodographs for each of the 6 regions (no rotation performed). Altitudes (km AGL) are indicated (0, 1, 3 and 6 km).

4. Summary and Conclusions

For the first time in Canada, this article uses a long period (1980 - 2020) of reanalyses (ERA5) proximity soundings and several convective parameters (Table A1) to characterize significant tornado (F/EF2$^+$) environments between Alberta to Quebec, Canada, and statistically compares the regional environments. Where possible, comparisons to other Canadian and international studies were made. After filtering 211 F/EF2$^+$ cases to prevent environment oversampling (based on Potvin et al. 2010), 166 events remained in the analysis (Fig. 1 and Table 1). Key results include:

1) ERA5-derived convective parameters are suitable to represent observed parameters, based on available rawinsonde comparisons.
2) Western Canada (Prairies) have nearly double the LCLs with higher LFCs in eastern Prairies compared to eastern Canada (southern Ontario/Quebec). This is due to more abundant boundary layer moisture and smaller dew point spreads in eastern regions.

3) Central North American continental regions have the most negative convective inhibition, mainly due to larger boundary layer dew point spreads, when comparing Canada and U.S. information, although variability is large.
4) Central Canada (Manitoba) has the largest mixed-layer CAPE, then falls off to the west and east, due to a combination of regional low level moisture differences and steeper mid-level lapse rates in western Canada.
5) Mean bulk wind shears and low level SRH increases from west to east, with eastern regions being significantly larger.
6) Based on Bunkers storm motion, eastern Prairie tornadic storms are predicted to be the most deviant (right movers), with eastern Canada being the least deviant.
7) Despite cold pool influences on tornadogenesis failure, western regions tend to have colder cold pools compared to eastern counterparts, based on the indices used.
8) The supercell composite and significant tornado parameters are generally less than U.S. magnitudes, particularly in western Canada, and would require recalibration; similar to most European events.
9) Central and eastern Prairie strong tornadic storms are dominated by thermodynamic influences compared to larger kinematic influences in eastern regions. Low- and mid-level vertical wind shears are particularly stronger in eastern Canada.
10) Related to (9), statistical analyses suggest a classification of Canadian tornado environments based on 2 general criteria: i) moisture regime and, ii) synoptic forcing. Manitoba clusters with Eastern Canada for the former, and with Western Canada for the latter.
11) Canonical correlation analysis suggests that the 6 regions (Fig. 1) are statistically distinct from each other, with respect to the 35 convective parameters used in this study.

Limitations of this work include: (1) limited sample sizes in each region; the robust statistical tests provide greater confidence in regional comparisons, and it is believed there are enough meteorologically representative cases in each region, although more would be valuable, (2) the use of provincial boundaries to group tornado events; future research will examine using cluster analysis or machine learning techniques, nonetheless, this study did show statistically significant regional differences, (3) all reanalyses have biases, timing and spatial errors (storm initiation, intensity and placement), and mesoscale effects that may not be captured (e.g. storm outflows, lake breezes, etc) (e.g. Allen and Karoly 2014; Gensini et al. 2014; Taszarek et al. 2018; King and Kennedy 2019); this study attempted to account for timing (and indirectly spatial) errors, however, more rigorous analysis would be required to address this issue.

Future work will, (1) compare strong and weak Canadian tornado environments and contrast these to other environments around the world, especially the U.S. and Europe, (2) examine more robust ways to group tornado environments in Canada, potentially utilizing cluster or machine learning techniques, (3) relate findings found herein (or from (1) and (2)) to synoptic patterns using synoptic typing techniques.

Acknowledgements

The authors thank Dr. David Sills (Northern Tornadoes Project (NTP) at Western University) for the tornado database as well as useful discussions, in collaboration with Dr. Julian Brimelow (Northern Hail Project (NHP) at Western University). Thanks to George Liu (formerly at CEOS) for producing some of the figures. For the ERA5 dataset, we acknowledge the Copernicus Climate Change Service, Climate Data Store, (2023): ERA5 hourly data on single levels from 1940 to present. Copernicus Climate Change Service (C3S) Climate Data Store (CDS), DOI: 10.24381/cds.adbb2d47. Thanks to Dave Carlsen (Storm Prediction Centre - Winnipeg) for useful supercell storm discussions. The research was supported financially and in-kind by a Natural Sciences and Engineering Research Council (NSERC) Discovery Grant and the NTP (to JH). The research of the second author was supported by the Polish National Science Center (grant no. 2020/39/D/ST10/00768).

Data Availability

All tornado reports used herein can be accessed via the Canadian tornado database (https://open.canada.ca/data/en/dataset/fd3355a7-ae34-4df7-b477-07306182db69) (Sills et al. 2012) as well as the Northern Tornadoes Project portal (NTP; https://ntpopendata-westernu.opendata.arcgis.com/). ERA5 can be accessed via the ECMWF Copernicus Climate Change Service (C3S) at https://cds.climate.copernicus.eu/.

Appendix A

The ERA5-derived convective parameters used to characterize F/EF2^{+} Canadian tornado environments (Table A1). The reader is referred to Taszarek et al. (2020) for detailed explanations and formulae for many of the parameters in Table A1.

Thermodynamic Parameters	**Definition / Description**
ML_CAPE	convective available potential energy, derived from the mixed-layer (0 - 500 m) parcel (J kg^{-1})
ML_03km_CAPE	convective available potential energy between surface and 3 km AGL, derived from the mixed-layer (0 - 500 m) parcel (J kg^{-1})
ML_CIN	convective inhibition, derived from the mixed-layer (0 - 500 m) parcel (J kg^{-1})
ML_LCL_HGT	height of the lifted condensation level, derived from the mixed-layer (0 - 500 m) parcel (m AGL)
ML_LFC_HGT	height of the level of free convection, derived from the mixed-layer (0 - 500 m) parcel (m AGL)
ML_MIXR	mixing ratio of the mixed-layer (0 - 500 m) parcel (g kg^{-1})
LR_03km	temperature lapse rate between 0 and 3 km AGL (K km^{-1})
LR_36km	temperature lapse rate between 3 and 6 km AGL (K km^{-1})
LR_24km	temperature lapse rate between 2 and 4 km AGL (K km^{-1})
Cold_Pool_Strength	difference between surface temperature and temperature of the downdraft (derived from DCAPE procedure) at the surface (K); DCAPE is initialized from 4 km AGL with a mean theta-e in 3–5 km AGL layer
Kinematic Parameters	**Definition / Description**
BS_01km	bulk wind shear between surface and 1 km AGL (m s^{-1})
BS_03km	bulk wind shear between surface and 3 km AGL (m s^{-1})
BS_06km	bulk wind shear between surface and 6 km AGL (m s^{-1})

BS_EFF	effective shear between parcel initialization height and half of the distance to equilibrium level height ($m\ s^{-1}$)
MW_01km	mean wind speed between 0 and 1 km AGL layer ($m\ s^{-1}$)
MW_06km	mean wind speed between 0 and 6 km AGL layer ($m\ s^{-1}$)
MW_13km	mean wind speed between 1 and 3 km AGL layer ($m\ s^{-1}$)
SRH_100m_RM	storm-relative helicity between surface and 100 m AGL for right-moving supercell vector ($m^2\ s^{-2}$)
SRH_500m_RM	storm-relative helicity between surface and 500 m AGL for right-moving supercell vector ($m^2\ s^{-2}$)
SRH_1km_RM	storm-relative helicity between surface and 1 km AGL for right-moving supercell vector ($m^2\ s^{-2}$)
SRH_3km_RM	storm-relative helicity between surface and 3 km AGL for right-moving supercell vector ($m^2\ s^{-2}$)
SV_500m_RM	streamwise vorticity between surface and 500 m AGL for right-moving supercell vector ($1\ s^{-1}$)
SV_01km_RM	streamwise vorticity between surface and 1 km AGL for right-moving supercell vector ($1\ s^{-1}$)
SV_03km_RM	streamwise vorticity between surface and 3 km AGL for right-moving supercell vector ($1\ s^{-1}$)
SV_FRA_500m_RM	streamwise vorticity fraction between surface and 500 m AGL for right-moving supercell vector (fraction)
SV_FRA_01km_RM	streamwise vorticity fraction between surface and 1 km AGL for right-moving supercell vector (fraction)
SV_FRA_03km_RM	streamwise vorticity fraction between surface and 3 km AGL for right-moving supercell vector (fraction)
Bunkers_RM_A	azimuth for a right-moving supercell vector. See Bunkers et al. (2000) for further details. (degrees)
Bunkers_RM_M	wind speed for a right-moving supercell vector. See Bunkers et al. (2000) for further details. ($m\ s^{-1}$)
Bunkers_MW_A	azimuth for mean (normal) storm motion vector. See Bunkers et al. (2000) for further details (degrees)
Bunkers_MW_M	wind speed for mean (normal) storm motion vector. See

	Bunkers et al. (2000) for further details (m s^{-1})
Composite Parameters	**Definition / Description**
Moisture_Flux_02km	mean wind speed multiplied by mean mixing ratio in the layer between surface and 2 km AGL (both) (g s^{-1} m^{-2})
ML_WMAXSHEAR	mixed-layer WMAX multiplied by surface to 6 km AGL bulk wind shear. See Taszarek et al. (2020) for further details on WMAXSHEAR. (m^2 s^{-2})
STP	significant tornado parameter based on the formula from Coffer et al. (2019) (unitless)
SCP	supercell composite parameter based on formula from Gropp and Davenport (2018), but with effective SRH replaced with surface to 3 km AGL SRH. This version uses effective shear and CIN terms. Based on the most-unstable parcel. (unitless)

Table A1: ERA5-derived convective parameters used to characterize F/EF2^+ Canadian tornado environments. (left column) the abbreviated parameter name used in the text, and (right column) parameter definition and any associated references (only for less common parameters). Explanations of most formulae used can be found in Taszarek et al. (2020).

Declaration of Generative AI and AIassisted technologies in the writing process:

During the preparation of this work the author(s) did not use any AI or AI-assisted technology during any stage of analysis or writing. The author(s) take(s) full responsibility for the content of the publication.

References

Allen, J. T., and D. J. Karoly, 2014: A climatology of Australian severe thunderstorm environments 1979-2011: Inter-annual variability and ENSO influence. *Int. J. Climatol.*, **34**, 81–97, https://doi.org/10.1002/joc.3667.

Anderson-Frey, A. K., Y. P. Richardson, A. R. Dean, R. L. Thompson, and B. T. Smith, 2016: Investigation of near-storm environments for tornado events and warnings. *Wea. Forecasting*, **31**, 1771–1790, https://doi.org/10.1175/WAF-D-16-0046.1.

Anderson-Frey, A. K., Y. P. Richardson, A. R. Dean, R. L. Thompson, and B. T. Smith, 2018: Near-storm environments of outbreak and isolated tornadoes. *Wea. Forecasting*, **33**, 1397–1412, https://doi.org/10.1175/WAF-D-18-0057.1.

Anderson-Frey, A. K., Y. P. Richardson, A. R. Dean, R. L. Thompson, and B. T. Smith, 2019: Characteristics of tornado events and warnings in the southeastern United States. *Wea. Forecasting*, **34**, 1017–1034, https://doi.org/10.1175/WAF-D- 18-0211.1.

Beebe, R. G., 1955: Types of airmasses in which tornadoes occur. *Bull. Amer. Meteor. Soc.*, **36**, 349–350, https://doi.org/10.1175/1520-0477-36.7.344.

Beebe, R. G., 1958: Tornado proximity soundings. *Bull. Amer. Meteor. Soc.*, **39**, 195–201, https://doi.org/10.1175/1520-0477-39.4.195.

Brimelow, J. C., J. M. Hanesiak and W. R. Burrows, 2011: Impacts of land-atmosphere feed-backs on deep, moist convection on the Canadian Prairies. *Earth Interact.*, **15**(31), 1-29, https://doi.org/10.1175/2011EI407.1.

Brooks, H. E., C. A. Doswell III, and J. Cooper, 1994: On the environments of tornadic and nontornadic mesocyclones. *Wea. Forecasting*, **9**, 606–618, https://doi.org/10.1175/1520-0434(1994)009<0606:OTEOTA>2.0.CO;2.

Brooks, H. E., J. W. Lee, and J. P. Craven, 2003: The spatial distribution of severe thunderstorm and tornado environments from global reanalysis data. *Atmos. Res*., **67-68**, 73–94, https://doi.org/10.1016/S0169-8095(03)00045-0.

Brooks, H. E., 2013: Severe thunderstorms and climate change. *Atmos. Res.*, **123**, 129–138, https://doi.org/10.1016/j.atmosres.2012.04.002.

Bullas, J.M. and A.F. Wallace, 1988: The Edmonton tornado, July 31, 1987. *Preprints, 15th Conf. On Severe Local Storms*, Baltimore, MD, Amer. Meteorol. Soc., 437-443.

Bunkers, M. J., B. A. Klimowski, J. W. Zeitler, R. L. Thompson, and M. L. Weisman, 2000: Predicting supercell motion using a new hodograph technique. *Wea. Forecasting*, **15**, 61–79, https://doi.org/ 10.1175/1520-0434(2000)015,0061:PSMUAN.2.0.CO;2.

Bunkers, M. J., 2018: Observations of right-moving supercell motion forecast errors. *Wea. Forecasting*, **33**, 145–159, https:// doi.org/10.1175/WAF-D-17-0133.1.

Charlton, R., B. Kachman, and L. Wojtiw, 1995: Urban hailstorms - A view from Alberta. *Nat. Hazards*, **12**, 29–75, https://doi.org/10.1007/BF00605280.

Cheng, V. Y. S., Arhonditsis, G. B., Sills, D. M. L., Auld, H., Shephard, M. W., Gough, Wm. A., & Klaassen, J., 2013: Probability of tornado occurrence across Canada. *J. Climate*, **26**, 9415-9428, https://doi.org/10.1175/JCLI-D-13-00093.1.

Chisholm, A.J. and J.H. Renick, 1972: The kinematics of multicell and supercell Alberta hailstorms. Hail Studies Report 72-2, Alberta Research Council, 24-31. [Available at Alberta Research Council, Edmonton, AB, T6H 5X2].

Coffer, B. E., and M. D. Parker, R. L. Thompson, B. T. Smith, and R. E. Jewell, 2019: Using near-ground storm relative helicity in supercell tornado forecasting. *Wea. Forecasting*, **34**, 1417–1435, https://doi.org/10.1175/WAF-D-19-0115.1.

Coffer, B. E., M. Taszarek and M. D. Parker, 2020: Near-Ground Wind Profiles of Tornadic and Nontornadic Environments in the United States and Europe from ERA5 Reanalyses. *Wea. Forecasting*, **35**, 2621-2638, https://doi.org/10.1175/WAF-D-20-0153.1.

Darkow, G. L., 1969: An analysis of over sixty tornado proximity soundings. *Preprints, Sixth Conf. on Severe Local Storms*, Chicago, IL, Amer. Meteor. Soc., 218–221.

Davies-Jones, R. P., 1984: Streamwise vorticity: The origin of updraft rotation in supercell storms. *J. Atmos. Sci.*, **41**, 2991–3006, https://doi.org/10.1175/1520-0469(1984)041<2991:SVTOOU>2.0.CO;2.

Davies-Jones, R. P., D. Burgess, and M. Foster, 1990: Test of helicity as a tornado forecast parameter. *Preprints, 16th Conf. on Severe Local Storms*. Kananaskis Park, AB, Canada, Amer. Meteor. Soc., 588–592.

Davies, J. M., 2004: Estimations of CIN and LFC associated with tornadic and nontornadic supercells. *Wea. Forecasting*, **19**, 714–726, https://doi.org/10.1175/1520-0434(2004)019<0714:EOCALA>2.0.CO;2.

Doswell, C. A. III, H. E. Brooks, and N. Doztek, 2009: On the implementation of the enhanced Fujita scale in the USA. *Atmos. Res.*, **93**, 554–563.

Dupilka, M. L. & Reuter, G. W., 2006a: Forecasting tornadic thunderstorm potential in Alberta using environmental sounding data. Part I: Wind shear and buoyancy. *Wea. Forecasting*, **21**, 325–335, https://doi.org/10.1175/WAF921.1.

Dupilka, M. L. & Reuter, G. W., 2006b: Forecasting Tornadic Thunderstorm Potential in Alberta Using Environmental Sounding Data. Part II: Helicity, Precipitable Water, and Storm Convergence. *Wea. Forecasting*, **21**, 336-346, https://doi.org/10.1175/WAF922.1.

Dupilka, M.L. and G.W. Reuter, 2011: Composite Soundings Associated with Severe and Tornadic Thunderstorms in Central Alberta. *Atmos.-Ocean*, **49**(3), 269-278, https://doi.org/10.1080/07055900.2011.607146.

Dyck, R., J. Hanesiak, N. Taylor, D. Sills, 2014: Tornadic Events During UNSTABLE: use of supplemental soundings. *27th Conference on Severe Local Storms*, 3–7 November, Madison, Wisconsin, Paper 24, 1-11. [Available at https://ams.confex.com/ams/27SLS/webprogram/Paper254167.html]

Edwards, R. and R. L. Thompson, 2000: RUC-2 supercell proximity soundings, Part II: An independent assessment of supercell forecast parameters. *Preprints, 20th Conf. on Severe Local Storms*, Orlando, FL, Amer. Meteor. Soc., 435–438.

Edwards, R., L. G. LaDue, J. T. Ferree, K. Scharfenberg, C. M. Maier, and W. L. Coulbourne, 2013: Tornado intensity estimation: past, present, and future, *Bull. Amer. Meterol. Soc*., **94**, 641-653. https://doi.org/10.1175/BAMS-D-11-00006.1.

Edwards, R., H. E. Brooks, and H. Cohn, 2021: Changes in tornado climatology accompanying the enhanced Fugita scale. *J. Appl Meteorol. Clim*., **60**, 1465-1482. https://doi.org/10.1175/JAMC-D-21-0058.1.

Etkin, D., S. E. Brun, A. Shabbar, and P. Joe, 2001: Tornado climatology of Canada revisited: Tornado activity during different phases of ENSO. *Int. J. Climatol.*, **21**, 915–938, https://doi.org/10.1002/joc.654.

Fawbush, E. J., and R. C. Miller, 1954: The types of air masses in which North American tornadoes form. *Bull. Amer. Meteor. Soc.*, **35**, 154–165, https://doi.org/10.1175/1520-0477-35.4.154.

Friendly, M. and J. Fox, 2021: candisc: Visualizing Generalized Canonical Discriminant and Canonical Correlation Analysis. R package version 0.8-6., https://CRAN.R-project.org/package=candisc

Gensini, V. A., T. L. Mote, and H. E. Brooks, 2014: Severe thunderstorm reanalysis environments and collocated radiosonde observations. *J. Appl. Meteor. Climatol.*, **53**, 742–751, https://doi.org/10.1175/JAMC-D-13-0263.1.

Gensini, V. A. and H. E. Brooks, 2018: Spatial trends in United States tornado frequency. *Clim. Atmos. Sci.*, **1**, 38, https://doi.org/10.1038/S41612-018-0048-2.

Gensini, V. A. and L. Bravo de Guenni, 2019: Environmental covariate representation of seasonal U.S. tornado frequency. *J. Appl. Meteor. Climatol.*, **58**, 1353–1367, https://doi.org/10.1175/JAMC-D-18-0305.1.

Gensini, V. A., C. Converse, W. S. Ashley, and M. Taszarek, 2021: Machine Learning Classification of Significant Tornadoes and Hail in the United States Using ERA5 Proximity Soundings. *Wea. Forecasting*, **36**, 2143-2160, https://doi.org/10.1175/WAF-D-21-0056.1.

Grams, J. S., R. L. Thompson, D. V. Snively, J. A. Prentice, G. M. Hodges, and L. J. Reames, 2012: A climatology and comparison of parameters for significant tornado events in the United States. *Wea. Forecasting*, **27**, 106–123, https://doi.org/10.1175/ WAF-D-11-00008.1.

Gropp, M. E. and C. E. Davenport, 2018: The Impact of the Nocturnal Transition on the Lifetime and Evolution of Supercell Thunderstorms in the Great Plains. *Wea. Forecasting*, **33**, 1045–1061, https://doi.org/10.1175/WAF-D-17-0150.1.

Hanesiak, J.M., R.L. Raddatz and S. Lobban, 2004: Local initiation of deep convection on the Canadian Prairie Provinces. *Boundary Layer Meteorol.*, **110**, 455–470, https://doi-org.uml.idm.oclc.org/10.1023/B:BOUN.0000007242.89023.e5.

Hanesiak, J. M. and others, 2011: Characterization and summary of the 1999-2005 Canadian Prairie drought. *Atmos.-Ocean*, **49**, 421-452, https://doi.org/10.1080/07055900.2011.626757.

Hersbach, H., and Coauthors, 2020: The ERA5 global reanalysis. *Quart. J. Roy. Meteor. Soc.*, **146**, 1999–2049, https://doi.org/10.1002/qj.3803.

Holm, S. 1979: A Simple Sequentially Rejective Multiple Test Procedure. *Scandinavian Journal of Statistics*, **6**, 65–70. http://www.jstor.org/stable/4615733.

Houston, A. L. and D. Niyogi 2007: The sensitivity of convective initiation to the lapse rate of the active cloud-bearing layer. *Mon. Wea. Rev.*, **135**, 3013–3032, https://doi.org/10.1175/MWR3449.1.

Insurance Bureau of Canada, cited 2018: Ottawa-Gatineau Tornadoes Cause $295 Million in Insured Damage. [Available at http://www.ibc.ca/on/resources/media-centre/media-releases/ ottawa-gatineau-tornadoes-cause-295-million-in-insured-damage].

Insurance Bureau of Canada, cited 2021: Barrie-and-area tornadoes insured damage increases to $100 million. [Available online at http://www.ibc.ca/on/resources/media-centre/media-releases/ Barrie-and-area-tornadoes-insured-damage-increases-to-100-million].

Johns, R. H., and C. A. Doswell III, 1992: Severe local storms forecasting. *Wea. Forecasting*, **7**, 588–612, https://doi.org/10.1175/1520-0434(1992)007<0588:SLSF>2.0.CO;2.

Johns, R. H., J. M. Davies, and P. W. Leftwich, 1993: Some wind and instability parameters associated with strong and violent tornadoes. Part II: Variations in the combinations of wind and instability parameters. *The Tornado: Its Structure, Dynamics, Prediction, and Hazards, Geophys. Monogr.*, No. 79, Amer. Geophys. Union, 583–590, https://doi.org/10.1029/GM079p0583.

Kerr, B. W. and G. L. Darkow, 1996: Storm-Relative Winds and Helicity in the Tornadic Thunderstorm Environment. *Wea. Forecasting*, **11**, 489–505, https://doi.org/10.1175/1520-0434(1996)011<0489:SRWAHI>2.0.CO;2.

King, P., M.J. Leduc, and B.P. Murphy, 1996: The climatology of tornadoes in southern Ontario: Possible effects of lake breezes. *Preprints, 18th Conf. on Severe Local Storms,* San Francisco, CA, Amer. Meteor. Soc., 627–630.

King, P., 1997: On the absence of population bias in the tornado climatology of southwestern Ontario. *Wea. Forecasting*, **12**, 939– 946, https://doi.org/10.1175/1520-0434(1997)012<0939:OTAOPB>2.0.CO;2.

King, P., M. J. Leduc, D. M. L. Sills, N. R. Donaldson, D. R. Hudak, P. Joe, and B. P. Murphy, 2003: Lake breezes in southern Ontario and their relation to tornado climatology. *Wea. Forecasting*, **18**, 795–807, https://doi.org/10.1175/1520-0434(2003)018<0795:LBISOA>2.0.CO;2.

King, A. T., and A. D. Kennedy, 2019: North American supercell environments in atmospheric reanalyses and RUC-2. *J. Appl. Meteor. Climatol*., **58**, 71–92, https://doi.org/10.1175/JAMC-D-18-0015.1.

Maddox, R. A., 1976: An evaluation of tornado proximity wind and stability data. *Mon. Wea. Rev.*, **104**, 133–142, https://doi.org/10.1175/1520-0493(1976)104<0133:AEOTPW>2.0.CO;2.

Markowski, P. N., J. M. Straka, E. N. Rasmussen, and D. O. Blanchard, 1998: Variability of storm-relative helicity during VORTEX. *Mon. Wea. Rev.*, **126**, 2959–2971, https://doi.org/10.1175/1520-0493(1998)126<2959:VOSRHD>2.0.CO;2.

Markowski, P. M., J. M. Straka, and E. N. Rasmussen, 2002: Direct surface thermodynamic measurements within the rear-flank downdrafts of nontornadic and tornadic supercells. *Mon. Wea. Rev.*, **130**, 1692–1721, https://doi.org/10.1175/1520-0493(2002)130<1692:DSTOWT>2.0.CO;2.

Markowski, P. N., J. M. Straka, C. Hannon, J. Frame, E. Lancaster, A. Pietrycha, R. Edwards, and R. Thompson, 2003: Characteristics of vertical wind profiles near supercells obtained from the Rapid Update Cycle. *Wea. Forecasting*, **18**, 1262–1272, https://doi.org/10.1175/1520-0434(2003)018<1262:COVWPN>2.0.CO;2.

Murdzek, S S., P. M. Markowski, Y. P. Richardson and R. L. Tanamachi, 2020: Processes Preventing the Development of a Significant Tornado in a Colorado Supercell on 26 May 2010, *Mon. Wea. Rev.*, **148**, 1753-1778, https://doi.org/10.1175/MWR-D-19-0288.1.

Newark, M. J., 1983: 1984: Canadian tornadoes, 1950–1979. *Atmos.–Ocean*, **22**, 343–353.

Oke, T. R., W. G. Bailey, and W. Rouse, 1998: *Surface climates of Canada*. McGill-Queen's University Press, ISBN 9780773563575, pp. 400.

Orf, L., R. Wilhelmson, B. Lee, C. Finley and A. Houston, 2017: Evolution of a long-track violent tornado within a simulated supercell. *Bull. Amer. Meteorol. Soc.*, **98**, 45-68, https://doi.org/10.1175/BAMS-D-15-00073.1.

Patil, I. 2021: Visualizations with statistical details: The 'ggstatsplot' approach. *Journal of Open Source Software*, **6**, 3167, https://doi.org/10.21105/joss.03167.

Peters, J. M., Brice E. Coffer, Matthew D. Parker, Christopher J. Nowotarski, Jake P. Mulholland, Cameron J. Nixon, and John T. Allen, 2023: Disentangling the Influences of Storm-Relative Flow and Horizontal Streamwise Vorticity on Low-Level Mesocyclones in Supercells. *J. Atmos. Sci.*, **80**, 129-149, https://doi.org/10.1175/JAS-D-22-0114.1.

Peterson, R. A., 2021: Finding Optimal Normalizing Transformations via bestNormalize. *The R Journal*, **13**, 310-329, https://doi.org/10.32614/RJ-2021-041.

Peterson, R. A. and J. E. Cavanaugh, 2020: Ordered quantile normalization: a semiparametric transformation built for the cross-validation era. *Journal of Applied Statistics*, **47**, 2312-2327, https://doi.org/10.1080/02664763.2019.1630372.

Pilguj, N., M. Taszarek, M. Kryza1, and H. E. Brooks, 2022: Reconstruction of Violent Tornado Environments in Europe: High-Resolution Dynamical Downscaling of ERA5. *Geophys. Res. Let.*, 1-12, https://doi.org/10.1029/2022GL098242.

Potvin, C., K. L. Elmore and S. J. Weiss, 2010: Assessing the Impacts of Proximity Sounding Criteria on the Climatology of Significant Tornado Environments. *Wea. and Forecasting*, **25**, 921-930, https://doi.org/10.1175/2010WAF2222368.1.

Raddatz, R. L. and J. D. Cummine, 2003: Inter-annual variability of moisture flux from the Prairie agro-ecosystem: Impact of crop phenology on the seasonal pattern of tornado days. *Boundary-layer Meteorol.*, **106**, 283-295, https://doi.org/10.1023/A:1021117925505.

Rasmussen, E. N. and D. O. Blanchard, 1998: A baseline climatology of sounding-derived supercell and tornado forecast parameters. *Wea. Forecasting*, **13**, 1148–1164, https://doi.org/10.1175/1520-0434(1998)013<1148:ABCOSD>2.0.CO;2.

Rasmussen, E. N. and J. M. Straka, 1998: Variations in Supercell Morphology. Part I: Observations of the Role of Upper-Level Storm-Relative Flow. *Mon. Wea. Rev.*, **126**, 2406–2421, https://doi.org/10.1175/1520-0493(1998)126<2406:VISMPI>2.0.CO;2.

Rasmussen, E. N., 2003: Refined supercell and tornado forecast parameters. *Wea. Forecasting*, **18**, 530–535, https://doi.org/10.1175/1520-0434(2003)18<530:RSATFP>2.0.CO;2.

Rodríguez, O., and J. Bech, 2020: Tornadic environments in the Iberian Peninsula and the Balearic Islands based on ERA5 reanalysis. *Intl. J. Clim.*, **41**, E1959-E1979, https://doi.org/10.1002/joc.6825.

Rotunno, R., and J. B. Klemp, 1985: On the rotation and propagation of simulated supercell thunderstorms. *J. Atmos. Sci.*, **42**, 271–292, https://doi.org/10.1175/1520-0469(1985)042,0271: OTRAPO.2.0.CO;2.

Sills, DM.L. and P. King, 2000: Landspouts at lake breeze fronts in southern Ontario. *Preprints, 20th Conf. on Severe Local Storms,* Orlando, FL, Amer. Meteor. Soc., 243–246.

Sills, D., V. Cheng, P. McCarthy, B. Rousseau, J. Waller, L. Elliott, J. Klaassen and H. Auld, 2012: Using tornado, lightning and population data to identify tornado prone areas in Canada. Extended Abstracts, *26th AMS Conference on Severe Local Storms*, Nashville, TN, Amer. Meteorol. Soc., Paper P59, 1-10. [Available at https://ams.confex.com/ams/26SLS/webprogram/Paper211359.html].

Sills, D. M. L, P. J. McCarthy and G. A. Kopp, 2014: Implementation and application of the EF-scale in Canada. *27th AMS Conference on Severe Local Storms*, Amer. Meteorol. Soc., Paper 16B.6, 1-8. [Available at https://ams.confex.com/ams/27SLS/webprogram/Paper254999.html].

Smith, S.B. and M.K. Yau, 1993a: The causes of severe convective outbreaks in Alberta. Part I: A comparison of a severe outbreak with two nonsevere events. *Mon. Weather Rev.,* **121**, 1099–1125, https://doi.org/10.1175/1520-0493(1993)121<1099:TCOSCO>2.0.CO;2.

Smith, S.B. and M.K. Yau, 1993b: The causes of severe convective outbreaks in Alberta. Part II: Conceptual and statistical analysis. *Mon. Weather Rev.,* **121**, 1126–1133, https://doi.org/10.1175/1520-0493(1993)121<1126:TCOSCO>2.0.CO;2.

Strong, G.S., 1979: Convective weather prediction based on synoptic parameters. *Preprints 11th Conf. Severe Local Storms*, Amer. Meteor. Soc., Kansas City, Missouri, Oct., 1979, 608-615.

Strong, G. S., 1986. Synoptic to mesoscale dynamics of severe thunderstorm environments: A diagnostic study with forecasting implications. Ph.D. thesis, University of Alberta, Edmonton, AB, 346 pp.

Strong, G.S., 1989: Limestone Mountain Experiment LIMEX-85. *Clim. Bull.*, **23**, 98-118.

Szoke, E. J., M. L. Weisman, J. M. Brown, F. Caracena and T. W. Schlatter, 1984: A subsynoptic analysis of the Denver tornadoes of 3 June 1981. *Mon. Wea. Rev.*, **112**, 790-808, https://doi.org/10.1175/1520-0493(1984)112<0790:ASAOTD>2.0.CO;2.

Taszarek, M., H. E. Brooks, and B. Czernecki, 2017: Sounding-derived parameters associated with convective hazards in Europe. *Mon. Wea. Rev.*, **145**, 1511–1528, https://doi.org/10.1175/MWR-D-16-0384.1.

Taszarek, M., H. E. Brooks, and B. Czernecki, P. Szuster, and K. Fortuniak, 2018: Climatological aspects of convective parameters over Europe: A comparison of ERA-Interim and sounding data. *J. Climate*, **31**, 4281–4308, https://doi.org/10.1175/JCLI-D-17-0596.1.

Taszarek, M., J. T. Allen, T. Pucik, K. A. Hoogewind and H. E. Brooks, 2020: Severe Convective Storms across Europe and the United States. Part II: ERA5 Environments Associated with Lightning, Large Hail, Severe Wind, and Tornadoes. *J. Climate*, **33**, 10263-10286, https://doi.org/10.1175/JCLI-D-20-0346.1.

Taszarek, M., N. Pilguj, J. T. Allen, V. Gensini, H. E. Brooks and P. Szuster, 2021: Comparison of Convective Parameters Derived from ERA5 and MERRA-2 with Rawinsonde Data over Europe and North America. *J. Climate*, **34**, 3211-3237, https://doi.org/10.1175/JCLI-D-20-0484.1.

Taszarek, M., Czernecki, B., & Szuster, P., 2023: ThundeR - a rawinsonde package for processing convective parameters and visualizing atmospheric profiles. *11th European Conference on Severe Storms*, Bucharest, 8-12 May, No. ECSS2023-28.

Taylor, N. M., D. M. L. Sills, J. M. Hanesiak, J. A. Milbrandt, C. D. Smith, G. S. Strong, S. H. Skone, P. J. McCarthy, J. C. Brimelow, 2011: The Understanding Severe Thunderstorms and Alberta Boundary Layers Experiment (UNSTABLE) 2008. *Bull. Amer. Meteor. Soc.*, **92**, 739-763, https://doi.org/10.1175/2011BAMS2994.1.

Thompson, R. L., R. Edwards, J. A. Hart, K. L. Elmore, and P. Markowski, 2003: Close proximity soundings within supercell environments obtained from the Rapid Update Cycle. *Wea. Forecasting*, **18**, 1243–1261, https://doi.org/10.1175/1520-0434(2003)018,1243:CPSWSE.2.0.CO;2.

Thompson, R. L., R. Edwards, J. A. Hart, K. L. Elmore, and P. Markowski and C. M. Mead, 2004: An update to the supercell composite and significant tornado parameters. *Preprints, 22nd Conf. Severe Local Storms*, Hyannis, MA, Amer. Meteorol. Soc., P8.1. [Available at https://ams.confex.com/ams/11aram22sls/techprogram/paper_82100.htm.]

Thompson, R. L., C. M. Mead, and R. Edwards, 2007: Effective storm-relative helicity and bulk shear in supercell thunderstorm environments. *Wea. Forecasting*, **22**, 102–115, https://doi.org/10.1175/ WAF969.1.

Thompson, R. L., B. T. Smith, J. S. Grams, A. R. Dean, and C. Broyles, 2012: Convective modes for significant severe thunderstorms in the contiguous United States. Part II: Supercell and QLCS tornado environments. *Wea. Forecasting*, **27**, 1136–1154, https://doi.org/10.1175/WAF-D-11-00116.1.

Thompson, R. L., B. T. Smith, A. Dean, and P. Marsh, 2013: Spatial distributions of tornadic near-storm environments by convective mode. *Electron. J. Severe Storms Meteor.*, **8**(5), http://www.ejssm.org/ojs/index.php/ejssm/article/viewArticle/125.

Warren, R. A., H. Richter, H. A. Ramsay, S. T. Siems, and M. J. Manton, 2017: Impact of Variations in Upper-Level Shear on Simulated Supercells. *Mon. Wea. Rev.*, **145**, 2659–2681, https://doi.org/10.1175/MWR-D-16-0412.1.

Warren, R. A., H. Richter, and R. L. Thompson, 2021: Spectrum of Near-Storm Environments for Significant Severe Right-Moving Supercells in the Contiguous United States. *Mon. Wea. Rev.*, **149**, 3299-3323, https://doi.org/10.1175/MWR-D-21-0006.1.

Wilcox, R. R. and T. Tian, 2011: Measuring Effect Size: A Robust Heteroscedastic Approach for Two or More Groups. *Journal of Applied Statistics*, **38**, 1359–1368, https://doi.org/10.1080/02664763.2010.498507.

Yuen, K. K. 1974: The Two-Sample Trimmed t for Unequal Population Variances. *Biometrika*, **61**, 165–170. https://doi.org/10.2307/2334299.

Zhang, C., M. Xue, K. Zhu and X. Yu, 2023: Climatology of Significant Tornadoes within China and Comparison of Tornado Environments between the United States and China. *Mon. Wea. Rev.*, **151**, 465-484, https://doi.org/10.1175/MWR-D-22-0070.1.

Zipser, E. J. and J. H. Golden, 1979: A summertime tornado outbreak in Colorado: Mesoscale environment and structural features. *Mon. Wea. Rev.*, **107**, 1328-1342, https://doi.org/10.1175/1520-0493(1979)107<1328:ASTOIC>2.0.CO;2.

Declaration of interests

☒The authors declare that they have no known competing financial interests or personal relationships that could have appeared to influence the work reported in this paper.

☐The authors declare the following financial interests/personal relationships which may be considered as potential competing interests: